SURFACE ENGINEERING AND CHARACTERIZATION OF LASER DEPOSITED METALLIC BIOMATERIALS

Sonia Samuel

Thesis Prepared for the Degree of

MASTER OF SCIENCE

UNIVERSITY OF NORTH TEXAS

May 2007

APPROVED:

Rajarshi Banerjee, Major Professor
Michael Kaufman, Committee Member and Chair of the Department of Materials Science and Engineering
Thomas Scharf, Committee Member
Nandika D'Souza, Graduate Programs Coordinator.
Oscar Garcia, Dean College of Engineering
Sandra L. Terrell, Dean of the Robert B. Toulouse School of Graduate Studies

Samuel, Sonia. *Surface Engineering and Characterization of Laser Deposited Metallic Biomaterials.* Master of Science (Materials Science and Engineering), May 2007, 74 pp, 6 tables, 31 figures, 27 references.

Novel net shaping technique Laser Engineered Net shaping™ (LENS) laser based manufacturing solution (Sandia Corp., Albuquerque, NM www.sandia.gov); Laser can be used to deposit orthopedic implant alloys. Ti-35Nb-7Zr-5Ta (TNZT) alloy system was deposited using LENS. The corrosion resistance being an important prerequisite was tested electrochemically and was found that the LENS deposited TNZT was better than conventionally used Ti-6Al-4V in 0.1N HCl and a simulated body solution. A detailed analysis of the corrosion product exhibited the presence of complex oxides which are responsible for the excellent corrosion resistance. In addition, the in vitro tests done on LENS deposited TNZT showed that they have excellent biocompatibility.

In order to improve the wear resistance of the TNZT system boride reinforcements were carried out in the matrix using LENS processing. The tribological response of the metal matrix composites was studied under different conditions and compared with Ti-6Al-4V. Usage of Si_3N_4 balls as a counterpart in the wear studies showed that there is boride pullout resulting in third body abrasive wear with higher coefficient of friction (COF). Using 440C stainless steel balls drastically improved the COF of as deposited TNZT+2B and seemed to eliminate the effect of “three body abrasive wear,” and also exhibited superior wear resistance than Ti-6Al-4V.

ACKNOWLEDGEMENTS

First, I would like to express my deep sense of gratitude to my graduate advisor Dr. Rajarshi Banerjee for his constructive ideas and constant support and guidance throughout the course of this work. His approach towards research and problem solving is something that I have learnt that would be an asset for my professional as well as personal life. As a mentor his appreciation was always been there which in turn enabled me to press forward and make substantial progress in my work. I am grateful to Dr. Thomas Scharf for his valuable inputs and guidance in the area of tribology. Also Dr Seifollah Nasrazadani and Dr Mohamed El Bouanani have been very generous in letting me use their lab facilities to conduct experiments. I would like to thank them as well. I would also like to thank my committee member and the department Chair Dr. Michael Kaufman for reviewing my work and for offering valuable suggestions during and after my defense. Dr Nandika D'Souza has been a great source of encouragement throughout my graduate program and I express my sincere gratitude to her.

My thanks is in so small measures for the help rendered by my colleagues Soumya Nag at Ohio State University and Anantha Puthucode in terms of processing and characterization. This work would not have been possible without the constant prayers and encouragement from my parents and my sister. I would also like to thank my friends Vaishali Paliwal, Anjana Rajendran, Kiran Chandran, Santosh Kumar, Gayatri Sunderasan and Maia Romanes for all their support throughout this work. The prayers of my dear friends at the Denton Bible Church have come a long way to see this work in to its completion and I express my whole hearted gratitude to them. Last but not the least, I consider the opportunity and ability to do this work as a great blessing from my savior and Lord Jesus Christ and I submit this work for HIS glory.

TABLE OF CONTENTS

Page

LIST OF TABLES

Page

LIST OF ILLUSTRATIONS

Page

CHAPTER 1

INTRODUCTION AND LITERATURE REVIEW

The most common and the most moveable joints in the body are the synovial joints, e.g., hip, knee or shoulder joints. These joints are complex in nature and can function under critical conditions of loading. The presence of the load–bearing connective tissue called the articular cartilage and a nutrient fluid called the synovial fluid within the joint area is responsible for the performance of these joints under load bearing conditions as shown in Fig.1.1. However these joints are prone to degenerative and inflammatory diseases that lead to pain and joint stiffness. Some of these degenerative processes affecting the synovial joints are osteoarthritis, rheumatoid arthritis (inflammation of synovial membrane), chondromalacia (softening of the cartilage) and normal ageing of the cartilage [1]. Statistics from the Centers for Disease Control and Prevention (CDC), National Institute of Arthritis and Musculoskeletal and Skin Diseases, shows that nearly 70 million people in the US have some form of arthritis or chronic joint symptoms and approximately 20.7 million adults in the United States have the most common form of arthritis, osteoarthritis, also called degenerative joint disease. Most persons over the age of 65 are affected with osteoarthritis in at least one joint, making this condition a leading cause of disability in the US [2].

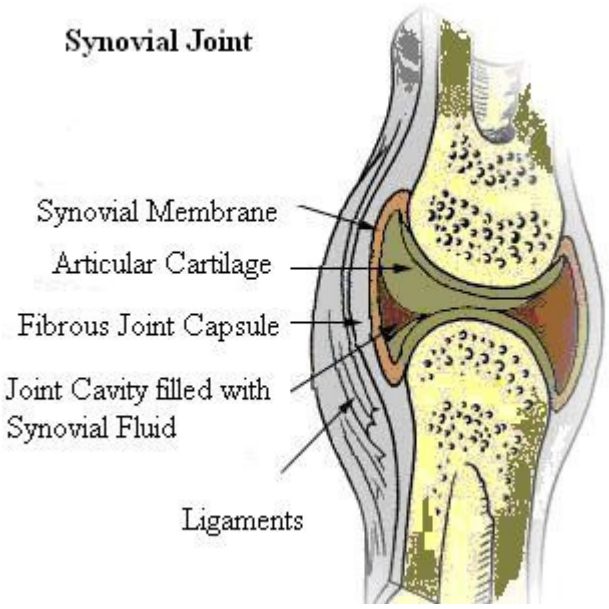

Figure1.1 Representation of a synovial joint.

Degeneration of these joints often requires surgical procedures to alleviate the pain and improve mobility. The orthopedic procedure adopted to replace these dysfunctional or arthritic joint surfaces with artificial materials is known as arthroplasty defined by the Dorland's Medical dictionary as 'plastic repair of a joint.' The total joint replacement arthroplasty has been one of the major breakthroughs in orthopedics. Total joint replacements (TJR) have now been a well established surgical technique involving a large number of knee and hip replacements every year. American Academy of Orthopedic surgeons report that as many as 418,000 partial and total knee replacements and 328,000 partial and total hip replacements(THR) are performed each year here in the United States. The modern artificial joint replacement procedure owes much to the work of John Charnley at Wrightington Hospital; his work in the field of tribology resulted in a design that completely replaced the other designs by the 1970s. However the higher wear rates associated with the artificial implant material leads to the formation of wear debris which

adversely effects the normal functioning of these prosthetic joints requiring a revision surgery to be performed on the patient [1]. Surgeons point out that these revision surgeries are much more difficult, may induce additional damage to the surrounding tissues, are much expensive and are less successful than the natural TJR surgeries. Consideration of these factors calls for an ideal biomaterial possessing the desired properties to make it a suitable replacement in a total joint replacement.

1.1 Desired Properties

1.1-1 Mechanical Properties

The performance of an 'ideal' biomaterial in a load bearing joint is attributed to an optimum combination of mechanical properties such as high strength, good ductility, good fatigue resistance, and low modulus [3]. As evident from the materials that has been used in the past decades (stainless steels UTS= 90 MPa to Ti-12Mo-6Zr-2Fe UTS= 1060 MPa) strength levels for orthopedic alloys are acceptable provided they have adequate ductility measured as percent elongation or percent area of reduction in standard tensile tests. Orthopedic implants are subjected to cyclic loading during body motion requiring them to possess excellent fatigue resistance. Factors like implant shape, design, processing, microstructure and type of loading condition make the determination of fatigue resistance a complex but an inevitable evaluation [1].

As far as the mechanical properties goes a growing concern that has been prevailing in the hunt for the 'ideal' biomaterial is to find a material which has a modulus value close to that of human bone (10-40 GPa). If the biomaterial has a significantly higher modulus than that of the bone coupled with variable fatigue resistance may lead to the failure of the prosthesis either by loosening or fracture. Lack of sufficient load transfer from the artificial implant to the bone leads

to bone resorption and subsequent loosening of the prosthetic device. Wolff's law ('The form being given, tissue adapts to best fulfill its mechanical function') points out that under the conditions of loading in joint prosthesis , the bone may show mass loss, reduced or decreased thickness resulting in osteoporosis. This phenomenon called stress shielding can eventually lead to the failure of the implant. Animal studies coupled with finite element analysis suggest that lower modulus prosthesis can reduce bone remodeling and better stimulate the natural femur in distributing the stress to the adjacent bone tissue. Attempts are being made in substituting implant materials with newer low modulus materials to reduce stress shielding and thereby prolonging the lifetime of the prosthetic device and hence eliminating the need for revision surgeries [1, 4].

1.1-2 Biocompatibility and Corrosion Resistance

In the selection of a material as a biomaterial one of the most important properties that it should possess is that it has superior biocompatibility and excellent resistance to degradation or corrosion resistance. The release of metal ions from the implant may lead to adverse body reactions and elicit allergic conditions in the surrounding tissues of the implant. These reverse conditions can be avoided by tailoring the composition of the implant material in a way that it does not result in the release of these toxic ions in the presence of body fluids. The release of these ions in turn depends on the corrosion rate of the alloy in the simulated conditions. Therefore much emphasis is laid on choosing a biocompatible and corrosion resistant material in joint prosthesis [1].

1.1-3 Wear Behavior

As the artificial implant continues to function as a substitute for the natural joint it tends to wear owing to its continuous rubbing to the adjacent parts resulting in debris generation. The debris thus formed interacts with the body fluids and tissues and leads to adverse reactions with in the body and is also associated in some extent to prosthetic loosening. Hence in addition to the above mentioned properties it is crucial that the implant material has good wear resistance with minimum debris generation. Thrust has been on selecting materials with good sliding and rolling wear resistance and optimizing a tribology design to better suit the conditions in the body.

1.2 Materials Used

Progress in total joint replacements was made possible by the efforts of G. K McKee and Sir John Charnley. The first metal-on-metal hip prosthesis constituted of stainless steel components. The low costs, ease of availability, ease of processing and good corrosion resistance made stainless steel a good candidate as an implant material. They are being used in temporary devices like fracture plates, screws, hip nails and THR stem. Owing to excessive friction and rapid loosening, Stainless steel was instantly taken over by a Co-Cr-Mo alloy. Though Co-Cr-Mo alloys exhibited better corrosion, fatigue strength and wear properties than Stainless steel the limitations in biocompatibility and modulus restricted the use of Co-Cr-Mo alloys in total joint replacements [1].

The 1940s witnessed the commercial development of titanium as an important metal finding applications as a structural material due to its high strength to weight ratio. In vitro studies carried out on titanium soon revealed that it has superior biocompatibility coupled with excellent corrosion resistance. Commercially pure titanium (C.P) exhibited better corrosion

resistance and tissue compatibility than stainless steel and was considered as a viable biomaterial. But the lower strength and poor wear resistance restricted the use of CP titanium to pacemaker cases, heart valve cages and reconstruction devices. Though CP is not a potential candidate for a TJR, cold working improved its strength and hence has been used as dental implants and maxillofacial applications [4].

Ti-6Al-4V ELI (extra low interstitial impurity content) originally developed for aerospace applications found a predominant position among TJR implants owing to high strength, low modulus, superior tissue compatibility and excellent corrosion resistance compared to previously used stainless steel and Co-Cr-Mo alloys. Currently it is being used in total hip/knee prosthesis, trauma fixation devices and dental implants. An alloy with a modified composition of Ti-3Al-2.5V has been used for femoral and tibial rods. However research in early 1980s revealed that the release of vanadium and aluminum ions in to the human system may result in potential neural disorders including peripheral neuropathy, osteomalacia and Alzheimer diseases. As a response to these concerns relating to vanadium and aluminum cytotoxicity newer orthopedic alloys like Ti-6Al-7Nb and Ti-5Al-2.5Fe were developed. These alloys though reduced the risk of potential toxicity due to vanadium still contained aluminum and had comparable mechanical properties including modulus as that of Ti-6Al-4V [4].

1.3 Beta Titanium Alloys

Further research in orthopedic alloys was directed in the development of alloys completely biocompatible and with a low modulus of elasticity. A major breakthrough that came along at this point of time is the development of β-titanium alloy characterized by higher strength, lower modulus and better toughness than the stainless steel, Co-Cr-Mo and α /β

titanium alloys. Compositionally they contain elements like zirconium, niobium, tantalum, molybdenum or iron considered being non toxic by nature [1, 3, 4].

Properties of some of these second generation β titanium alloys are tabulated and discussed in the paragraphs to follow. One of the earlier alloys to be developed in this class of alloys was Ti-12Mo-6Zr-2Fe (TMZF). This alloy received the approval from Food and drug administration (FDA) to be used in certain orthopedic products. TMZF alloy is a metastable alloy retaining an all β structure followed by rapid cooling from its β transus of 754^0 C or higher. Upon subsequent ageing fine scale α phase is precipitated. The all β structure is characterized by excellent strength and ductility, low modulus of elasticity coupled with good fracture toughness and better wear resistance much superior than that of Ti-6Al-4V [4].

Ti-13Nb-13Zr alloy developed by Smith and Nephew Richards Inc. was reported to be a near β alloy with the presence of hcp martensite (α') in the water quenched condition. On subsequent ageing submicroscopic bcc β precipitates along with the hcp martensite (α') contributing to the hardening of the material. In the aged condition this alloy exhibits good strength and low modulus and higher toughness than that of Ti-6Al-4V alloy and hence found application as an orthopedic alloy. Ti-15Mo-3Nb-3O alloy developed by TIMETAL Inc. in the 80s though originally developed as a matrix material for metal matrix composites owing to its higher tensile strength and lower modulus of elasticity was used as an orthopedic alloy. The oxygen level in this alloy was increased to enhance the α stabilization. Tiadyne 1610 developed by Teledyne Wah Chang Albany (TWCA) with niobium and hafnium as alloying elements also exhibited low modulus and high tensile strength making it an eligible candidate for use in orthopedics [4].

Ti-15Mo developed by Synthes USA is a metastable β alloy retaining its β structure after solution annealing at 800^0 C followed by subsequent rapid quenching. Along with superior tensile strength comparable to Ti-6Al-4V and CP Ti and lower modulus this alloy showed good corrosion resistance. Other alloys that were added to this class of low modulus, biocompatible β alloys were Ti-15Zr-4Nb-2Ta-0.2Pd, Ti-15Sn-4Nb-2Ta-0.2Pd.

With the intention of achieving the dual requirement of low modulus, approaching that of bone and enhanced biocompatibility, synthesis of metastable beta titanium alloy systems has been in progress over the past decade. H. J Rack et al. at the Clemson University and J. Silvestri et al. at Teledyne Allvac inc. developed the Ti-Nb-Zr-Ta system (TNZT) alloys which exhibited the lowest modulus value of 55GPa so far, in close comparison to that of the bone (10-40 GPa) [5]. Apart from the advantage of having a low modulus value this system minimizes potentially adverse tissue reactions through the restricted use of 'biocompatible' Nb, Ta and Zr and also maintains adequate strength [1]. In addition to these advantages their fatigue behavior is comparable to that of other beta titanium alloys i.e. $\sigma_{limit} = 0.5\ \sigma_{yield.}$ During the same period Niinomi et al. from Tohayashi University, Japan developed a similar alloy based on the TNZT system. The alloy developed had a composition of Ti-29Nb-13Ta-4.6Zr. The development of this alloy system by this group was largely influenced by the reports from Steinemann et al. who conducted cytotoxicity studies on pure metals and their relationship between biocompatibility and polarization resistance of typical pure metals and surgical implants materials. The results show high cytotoxicity of V and tissue response of scar type tissue due to Al, while Ti, Nb, Ta and Zr exhibit excellent biocompatibility. The tensile strength and elongation of this alloy was also equivalent or greater than those of conventional Ti alloys for implant application. The

Young's modulus value reported was also of the order of 55GPa quite lower when compared to the Ti-6Al-4V ELI. [6].

The following table, Table 1.1 summarizes the mechanical properties of the orthopedic alloys developed/utilized as orthopedic implants [1].

Alloy	Modulus (GPa)	Yield Strength(MPa)	UTS(MPa)	Comments
Co-Cr-Mo	200-230	275-1585	600-1795	Very High Modulus, High Strength
Stainless steel (316 L)	200	170-750	465-950	Very High Modulus, High Strength
C.P Ti	105	692	785	High Modulus, Moderate Strength
Ti-6Al-4V	110	850-900	960-970	High Modulus, High Strength
Ti-35Nb-7Zr-5Ta	55	530	590	Low Modulus, Low Strength
Ti-35Nb-7Zr-5Ta LENS™	55	813	834	Low Modulus, High Strength
Bone	10-40		90-140	

Table 1.1: Mechanical properties of orthopedic alloys developed/utilized as orthopedic implants.

1.4 Design and Processing

Orthopedic femoral implants have a complex geometry with different property requirements at different locations. As shown in Fig. 1.2 the femoral ball or the femoral head requires enhanced wear resistance on the surface while maintaining the fracture toughness of the core. On the other hand the femoral stem should be such that it has to be characterized by high strength, low modulus, good fatigue resistance and excellent adhesion to the bone tissue referred to as osseo integration. Hence owing to their poor wear resistance the applications of Ti alloys as

femoral heads has been restricted and instead ceramics (Alumina or Zirconia) or Co-Cr alloys have been used. Even though these materials offer excellent wear resistance their poor fracture toughness leads to the failure of these femoral heads while in use there by requiring revision surgeries. Also the use of ceramics as femoral heads leads to an undesirable metal/ceramic interface. This can be avoided by using metal matrix composites as femoral heads, which will subsequently improve the wear resistance and also maintain the fracture toughness of the core. Since, β Ti alloys, such as TNZT are expected to become the new generation alloys for implant applications, the present study focuses on the development of composites based on these alloys as matrices. These site specific property requirements calls for a manufacturing technique that could process a functionally graded integrated implant. [7-9].

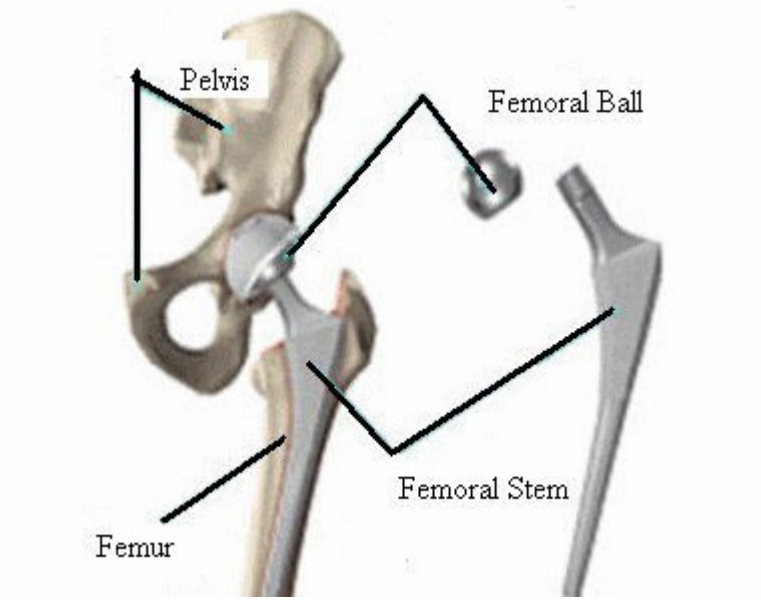

Figure 1.2 Femoral implant.

1.4-1 Laser Engineered Net Shaping.

Past decades have witnessed the evolution of rapid prototyping techniques like stereo lithography in the manufacturing sector. These methods are based on designing a three dimensional component using computer aided design and layering this information and transferring it to a computer controlled manufacturing system to reconstruct the component in a layer by layer fashion. However Stereolithography is predominantly used for polymer and polymer coated materials. The fabrication of metallic components using the solid free form fabrication route has been one of the major breakthroughs in manufacturing technology. The layer glaze process developed by the United Technologies Research Center (UTRC) was a pioneering work in rapid prototyping. Bulk metallic components of near net shape were manufactured by depositing multiple thin layers using an energy beam. Energy beam used was laser and the material was fed in the form of powders or wires. [10]

The advent of these two processing techniques viz. Stereolithography and layer glaze saw the development of new generation of processes for laser deposition. These include Laser Engineered Net shaping™ (LENS) laser based manufacturing solution (Sandia Corp., Albuquerque, NM www.sandia.gov) and directed light fabrication (DLF). The LENS process was originally developed by Sandia National Laboratories and later refined and commercialized by Optomec Design Company of Albuquerque, New Mexico. [10]. These machines deposit powders in parts or patterns dictated by computer aided design (CAD) files. A Nd: YAG high powered laser is used to create a melt pool on a metallic substrate, metal powder is blown in through a nozzle assembly into the pool thereby increasing the material volume as shown in Fig.1.3. This process is repeated over and over again as specified by the computer aided design (CAD) file to form a metal version of the CAD model. The deposition of the metal component is

done in a closed work space called the glove box in which an argon atmosphere is maintained thereby controlling the oxygen level in the ranges of less than ten parts per million [11].

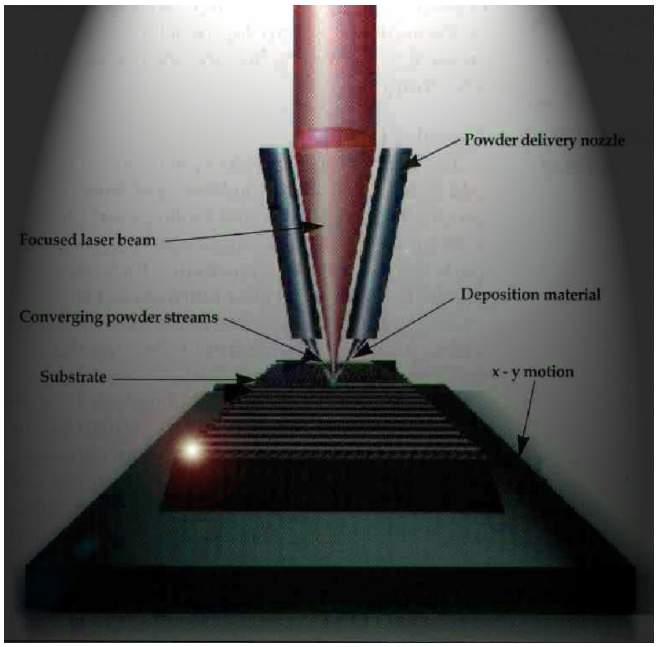

Figure 1.3 Molten metal deposition on the substrate.

The materials deposited using LENS undergo rapid solidification and thereby result in the formation of fully dense metals with excellent hardness, strength and ductility. Studies confirm that these material properties exceed that of wrought materials. These excellent properties are due to the result of the fine scale microstructure owing to the rapid solidification. Moreover, when compared to the conventional processing techniques such as forging and machining LENS is an additive manufacturing process. The nozzles deposit almost the exact amount of material required thereby reducing machining and cleaning to a larger extent when compared to the conventional techniques.

Another advantage that goes without mentioning is the ability to rapidly and efficiently manufacture custom-designed implants. The major advantage of using this novel near-net shaping process in processing an implant is its ability to functionally grade a deposit. The

orthopedic implants are geometrically quite complex and require different property requirements at different sites. The use of LENS processing technique could be exploited in manufacturing these implants with site specific property requirements. Also LENS process uses the flexibility of using powder feedstock allowing the flexibility of depositing blends of elemental powders to create alloys in situ. This provides with the advantage of depositing homogenous alloys and metal-matrix composites with refined microstructures using LENS hence reducing the requirements for further thermo mechanical processes [12].

1.5 Specific Issues Addressed in Literature on Beta Titanium Alloys

As discussed earlier an ideal recipe for a material to be used as orthopedic implant is that it exhibits excellent biocompatibility with absolutely no adverse tissue reactions, good corrosion resistance, adequate mechanical strength, low modulus comparable to that of the bone and good wear resistance. The following section discusses some of the specific issues addressed in the literature on Beta titanium alloys.

1.5-1 Corrosion Resistance

In order to facilitate a comparison between pure metals and alloys used in the implant industry an investigation on their corrosion resistance was carried out by Zitter et al. The materials tested were Au, Fe Cr Ni, Co Cr W Ni, Ti, Ti-6Al-4V, CP Ti, Nb and Ta. Electrochemical tests were carried out at 37^0 C in a concentration cell with standard calomel electrode as the reference electrode. The redox nature of a series of solutions including pure saline, pure saline deaerated with Nitrogen and tissue culture fluid was assessed using potentiodynamic measurements and it was found that the resting potential of the tissue culture

fluid (=simulated body fluid) resembles more closely to that of saline solution and hence all tests were carried out in the deaerated saline solution. The results indicate that in stable redox system gold, stainless steels, Co alloys exhibited highest current densities 35.8, 2.28, 3.0 $\mu A/cm^2$, where as Ti, Ti-6Al-4V, Nb and Ta exhibited an anodic current density in the range of 0.022 to 0.007 $\mu A/cm^2$. The low anodic current densities are an indication of the passivation behavior of these materials thereby suggesting that they have good corrosion resistance when compared to the other conventional metallic systems [13].

A study on Beta and near Beta alloys on their corrosion resistance was carried out by D Velten et al. The materials tested were Ti-13Nb-13Zr, Ti-15Mo-5Zr-3Al, Ti-30-Nb, Ti-30Ta and Ti-6Al-4V. The tests were carried out in 0.5 molar H_2SO_4 using Pt as the counter electrode. The range of passivity with a quite constant current density of the order of 0.01 $\mu A/cm^2$ extends from about 0 to 1600 mV. Potentials of about 300-500 mV typical of 316 L Stainless steels and Co Cr Mo alloys could be easily reached in the body in the case of inflammation. This indicates that the corrosion resistance of these beta and near beta alloys are superior to stainless steel and Co Cr Mo alloys are comparable to that of Ti-6Al-4V [14].

Corrosion resistance measurements were carried out by Y.L Zhou et al. on Ti-Ta alloy system in comparison with CP Ti and Ti-6Al-4V. The alloys were tested in 5 % HCl solution and the potential was measured with reference to a standard calomel electrode. The critical current densities and passive current density and primary passivation potentials of the Ti-Ta alloys were similar to that of the CP Ti and Ti-6Al-4V alloys. The E_{br}, breakdown potential values of two of the compositions studied Ti-30%Ta and 70 %Ta showed a significant increase and a decrease in current densities indicative of the fact that these alloy compositions shows better corrosion resistance when compared to the other alloys studied [15].

Ti-12Mo-6Zr-2Fe alloy a beta titanium alloy developed for surgical implants was evaluated for its corrosion resistance and compared with Ti-6Al-4V by a group at Howmedica Inc. Anodic polarization testing was carried out on both the above alloys in deaerated saline solution (0.9 % NaCl) at 37^0 C. The results of this study indicate that as the potential is increased each alloy reaches a stable passive current density. After a potential of +1000 mV vs. SCE further increase of potential does not result in any increase in current density exhibiting the presence of a protective oxide layer and that the breakdown of this layer is does not take place even at this excessive polarization [16].

1.5-2 Borides as Reinforcement

Titanium and their alloys are characterized by low density, excellent corrosion resistance and high mechanical strength when compared to other structural metals and alloys. However their applicability is limited due to their poor tribological properties. Their poor tribological functionality is directly related to its low c/a ratio as a HCP metal. As discussed earlier a femoral implant has a complex geometry and has site specific property requirements. The femoral ball which is in sliding and rotational motion within the joint is required to exhibit better wear resistance when compared to the femoral stem. Sliding wear properties of TiB/Ti-6Al-4V metal matrix layer fabricated using laser cladding and Laser melt injection evaluated in a previous study by De Hosson et al. shows improved tribological properties of this layer. The characteristic boride morphologies namely the eutectic and primary borides were formed by changing the laser cladding conditions that determines the cooling rates. The wear test was carried out in this case using a pin-on disk set up at two different loads and the specific wear rates and coefficient of friction established. The results show that the general trend of the wear behavior was such that

after some incubation and subsequent transition period, a constant wear rate was established. In the case of the metal matrix coating consisting of primary borides the wear rate is found to be higher for lower loads and lower for higher loads. The same trend is observed in the metal matrix coatings with eutectic borides. The microstructural evidence of these metal matrix layers shows that these layers exhibit excellent interfacial bonding between the primary TiB and the eutectic TiB particles. This explains uniform wear behavior prevalent in these layers. The summary of the wear studies reported in this study highlights the excellent wear resistance of the Laser engineered TiB/Ti-6Al-4V MMC layers [17].

1.5-3 Wear Resistance

Current generation of metastable β alloys though exhibit attractive mechanical and physical properties generally show poor fretting and wear resistance. Frictional behavior of some selected orthopedic biomaterials has been studied by H. J Rack and M. Long. The four titanium alloys studied were Ti-35Nb-8Zr-5Ta with slightly different compositions (TNZT and TNZTO), a metastable β alloy (21SRX) and Ti-6Al-4V ELI. The test set up was based on reciprocating-sliding pin on flat test stations. Two apparent contact stressed 1.5 and 5 MPa were chosen and tests were conducted at a 25 mm stroke rate. The materials to be tested were fabricated in the form of pins and were made to slide across a counterpart material. The counterpart material chosen was high strength maraging steel with a hardness of 58HRc which was selected owing to its high wear resistance. A thorough analysis of the surface morphology was carried out using SEM/EDS after the wear test. The dry frictional response of these alloys tested showed a dependence on cyclic count, sliding velocity and alloy phase structure. All of the alloys tested exhibited an initial run in period followed by a steady state behavior. The coefficient of friction

values for TNZT alloys at low contact stresses was observed to depend on sliding velocity, this dependence was not prominent at high contact stresses and the other alloys tested. The steady state dynamic coefficient of friction values for the metastable β titanium alloys were always higher than that of Ti-6Al-4V under all conditions of contact stresses tested. Worn surfaces showed extensive plastic deformation, micro-plowing, micro-cracking perpendicular to the sliding direction, shear delamination and smearing with the transfer of the counterpart material. The surface roughness analysis showed that the roughness of the metastable Ti alloys tested were higher than that for Ti-6Al-4V [18].

Wear resistance of Ti-29Nb-13Ta-4.6Zr in comparison with Ti-6Al-4V was studied by Niinomi et al. The TNZT alloy was heat treated to different conditions to study the effect of heat treatment on wear resistance of these alloys. The test set up used was a pin-on-disc one with the material to be tested fabricated as a pin and the counter face material chosen were Stainless steel (88.5 HRB), pig bone and UHMWPE. The test was conducted under a normal load of 3N in 0.9% NaCl. The wear loss measurements indicate that heat treatment is not a practical way to improve the wear resistance of the titanium alloys. The TNZT and the Ti-6Al-4V alloys were then subjected to thermal oxidation to study the effect of an oxide layer on these alloys. Results indicate that the presence of an oxide layer greatly improves the wear resistance of TNZT alloys while it has practically no effect on Ti-6Al-4V. The effect of counter face materials were prominent in the case of both the alloys tested. Sliding on Stainless steel results in more wear loss for both the alloys when compared to UHMWPE and pig bone. The TNZT oxidized condition exhibited excellent wear resistance regardless of the counter face material [19].

1.5-4 Biocompatibility

Biocompatibility and corrosion resistance is one of the key properties that a material being considered as a biomaterial should possess. Local adverse tissue reactions owing to metal ion release may result in allergic reactions requiring revision surgeries. Okazaki et al. performed a study in which they evaluated the metal ion releases from Stainless steels, Co-Cr alloys, titanium and titanium alloys in simulated body fluids and in rat tibia tissues. The results show a higher corrosion resistance of Ti and its alloys attributed to the passive film on their surface. Reports from Hanawa et al. confirmed that the repassivation reaction in titanium was of the order of 30 ms in Hanks solution which is considered to be very rapid [20].

Cytotoxicity testing is an inexpensive means to determine whether a material contains extractable that are harmful to the human biological system and is being used to evaluate the biocompatibility of implant materials. Ti-Ta a Beta titanium alloy and pure titanium was subjected to cytotoxicity studies by Niinomi et al. The metallic specimens were autoclaved in Eagles Culture solutions at body temperature and then extracted after 7 and 14 days. The extracted solution was then analyzed for cytotoxicity by evaluating the survival rate of L-929 cells derived from mice using MTT method. MTT method evaluates the cell respiration by the mitochondria. The results indicate that the cell viability of the studied Ti-Ta alloys is very much comparable to that of pure titanium [15].

Cell viability studies on Ti-29Nb-13Ta-4.6Zr, Ti-6Al-4V and CP titanium was carried out by the same group Niinomi et al. by the same technique outlined above. The results of the study was that the cell viability of Ti-29Nb-13Ta-4.6Zr is almost the same as that of pure Ti and greater than that of the currently used Ti-6Al-4V. Thus it was concluded that Ti-29Nb-13Ta-4.6Zr was less cytotoxic when compared to Ti-6Al-4V. The amount of wear debris formed also

determines the cytotoxicity and hence it is important that the material chosen exhibit excellent wear resistance [21]. Surface modification of the implant material has been considered as a viable option to improve the biocompatibility of these implants materials. Induction of calcium phosphate based materials on the surface of titanium to improve oseoinduction has been researched in the past years [20]. Varying the surface roughness on titanium substrates and their subsequent response in rat bone marrow cells have been evaluated by J. van den Dolder et al. [22].

1.6 Specific Issues Addressed in this Work

As evident from the literature review the quest for a suitable implant material with the suitable property requirements have led researchers to an alloy system of Ti-35Nb-7Zr-5Ta. Previous research on laser-deposited materials depicts that these materials exhibit a substantially refined microstructure as compared to their conventionally processed (e.g. ingot processing) counterparts. As a prerequisite to qualify as a potential candidate for implant applications, it is required that the material exhibit superior corrosion resistance and biocompatibility. In this work the biocompatibility and the corrosion resistance of the LENS deposited TNZT alloys are investigated and are compared with the currently used Ti-6Al-4V ELI (extra low interstitial) alloy. Furthermore, since biomedical implants are geometrically quite complex, employing novel near-net shape processing technologies, such as LENS, it becomes possible to not only rapidly and efficiently manufacture custom-designed implants but also to functionally-grade them to exhibit required site-specific properties. For e.g. the sliding and rolling wear resistance is of primary importance to a material that is being used as a femoral head in a femoral hip implant. Using the laser-engineered net shaping (LENS) process, it has been

successfully demonstrated that *in situ* TiB reinforced Ti alloy composites can be fabricated in a single step. The reinforcement of Ti alloys with TiB has been studied previously and has been known for its excellent tribological response. Therefore, the current effort in this work is directed towards the laser-deposition of boride reinforced TNZT composites based on the nominal matrix composition Ti-35Nb-7Zr-5Ta (all in wt %).There is a need to study the fundamental tribological properties and mechanisms of these next generation alloys before application. Sliding wear resistance and friction behavior was examined under a wide range of post processing and testing conditions such as varying the concentrated interfacial load, the effect of ex situ annealing on the tribological properties, and the role of counterpart material. Correlating the tribological properties to the surface microstructure was also studied under these conditions.

CHAPTER 2

PROCESSING AND CHARACTERIZATION TECHNIQUES EMPLOYED

This chapter discusses the experimental techniques and methods adopted in the processing of Ti-35Nb-7Zr-5Ta (TNZT) alloys and their testing and subsequent characterization. The processing technique employed is Laser Engineered Net shaping™ (LENS) laser based manufacturing solution (Sandia Corp., Albuquerque, NM www.sandia.gov), the details of which are discussed in the sections to follow. The LENS processed TNZT alloys were then tested for their corrosion resistance using a flat cell PARSTAT potentiodynamic set up. The oxide layer formed as a result of corrosion was subjected to microstructural characterization using scanning electron microscope, FEI Nova 200 Dual-beam FIB. Surface analytical studies were performed on the oxide layer using X-ray photo spectroscopy to determine the compositions of the oxides. Surface topography of the oxide layer was analyzed using atomic force microscopy.

Boride reinforcement on the softer β TNZT was also carried out using LENS. The Borides thus formed were examined microscopically to get an insight into their evolution at a microstructural level. The boride reinforced alloys were then tested for their wear resistance using a ISC Falex Pin-on-Disk Tribometer. Heat treatments were carried out in a programmable furnace and their subsequent wear response was studied. In order to predict the wear mechanisms the wear tracks were examined microscopically under a Scanning electron microscope.

2.1 Processing Technique

2.1-2 Laser Engineered Net Shaping (LENS)

The LENS process uses a design file in the computer aided design (CAD) format which is then sliced using LENS Part prep software to 2D layers, with information about each layer.

This sliced file is then converted to a machine coded file of DMC format. A high powdered pulsed Nd: YAG laser with a power rating of (760W) emitting near infrared laser radiation of a wavelength of 1.064 μm is used to create a melt pool on a metallic substrate. The LENS unit used for these depositions was designed by Sandia National laboratories and is now commercialized by Optomec Inc. is shown in Fig. 2.1. In this case for the deposition of TNZT alloys, a Ti-6Al-4V (Manufactured by TIMET Inc.) substrate was used. The powder is fed through a powder feeder which is carried by an inert gas into a multi nozzle powder feeder assembly. The in situ alloys were deposited from an elemental blend of pure Ti, Nb, Zr and Ta powders mixed in the ratio of 53 wt% Ti+ 35 wt% Nb + 7 wt% Zr + 5 wt% Ta. The elemental powder feed stock used for this deposition are as follows.

Ti: 99.9 % pure; -150 mesh (Provided by Alfa Aesar)

Nb: 99.9 pure; -200 + 325 mesh (Provided by Reading alloys)

Zr: 99.8 % pure; -140 + 325 mesh (Provided by CERAC Specialty)

Ta: 99.98 % pure; -100 mesh (Provided by Alfa Aesar).

In the case of deposition of TNZT with boride reinforcements the elemental blend composition was Ti, Nb, Zr and Ta powders mixed in the ratio of 51 wt% Ti+ 35 wt% Nb + 7 wt% Zr + 5 wt% Ta + 2wt% B. The laser power used for these depositions were 350 W. The hatch width for this deposition was of the order of 0.38 mm, the layer speed was 0.25 mm and the travel speed was 635mm/min. A cylindrical geometry was preferred to facilitate further testing with a diameter of 12mm and a height of 30 mm.

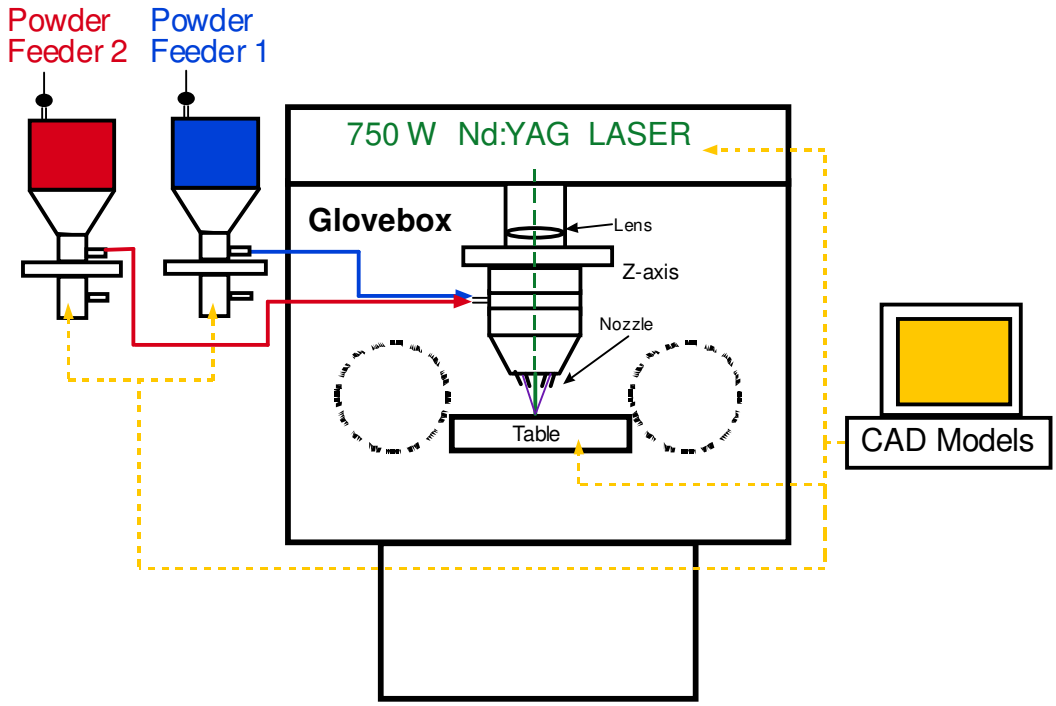

Figure 2.1 Schematic diagram of the LENS process.

2.2 Testing Techniques

2.2-1 Wear Testing

Friction and wear behavior of TNZT+2B and Ti-6Al-4V ELI (Extra Low Interstitial) were determined using a Falex (Implant Sciences) ISC-200 Tribometer. This tribometer is a pin-on-disk type configuration which measures the sliding friction coefficients on planar surfaces. A vertical (normal) load was applied to generate a point contact between the pin and the disk surfaces. The pin counter face materials were held stationary by a cantilever beam while the alloy disk samples were rotated under it. The counter face materials chosen were Si_3N_4 (H= 1550 HV/10) and SS 440 C (H= 420 HV/10) balls of 1.6 mm radius. Tests were performed at a constant normal load of 5 N which corresponds to the initial mean Hertzian contact stress (p_m) values. The friction coefficients were calculated throughout the test by taking the ratio of the

tangential load, measured by a strain gauge transducer, to the normal load. The tests were performed up to 10,000 sliding cycles at a tangential sliding velocity of 46 mm/s, which lies in the range typically found in hip joints [24], In addition, the tests were run at room temperature in open air with a relative humidity of ~35 %. Before testing the 15 mm diameter alloy surfaces were polished to # 1200 SiC followed by fine polishing up to 0.05 μm colloidal silica. Also, some of the polished samples were subjected to separate heat treatments in air before testing, shown in Table 2.1 The objective of the TNZT+2B and the Ti-6Al-4V ELI alloy heat treatments were two fold, to study the influence of α precipitates and the influence of the oxide layer, formed as a result of the heat treatment, on the friction and wear behavior.

ALLOY	**HEAT TREATMENT**
Ti-6Al-4V ELI	As deposited
Ti-6Al-4V ELI	600^0 C/10hours/FC/Oxide Layer
Ti-6Al-4V ELI	600^0 C/10hours/FC/Oxide Layer removed
TNZT 2B	As deposited
TNZT 2B	600^0 C/10hours/FC/Oxide Layer
TNZT 2B	600^0 C/10hours/FC/Oxide Layer removed

Table 2.1: Heat treatment conditions for Ti-6Al-4V and TNZT 2B for wear testing.

2.2-2 Potentiodynamic Testing

Principle:

Corrosion is a process involving electrochemical oxidation and reduction reactions. Hence electrochemical methods can be used to study and measure corrosion response of a system. Immersion of a metal in a solution results in electrochemical reactions characteristic of the metal-solution interface at the surface of the metal resulting in the corrosion of the metal. These electrochemical reactions create an electrochemical potential called the corrosion potential or the open circuit potential. This potential is determined by the specific chemistry of the system and hence is a characteristic of the metal-solution system. As in the case of all voltage measurements, corrosion potential of E_{CORR} is measured as potential energy difference with a reference system. A saturated calomel electrode is used as a reference electrode.

A typical corrosion measurement system consists of a test cell with a metal specimen (working electrode) immersed in the solution in which the corrosion resistance has to be measured. A reference Electrode contacts the solution through a bridge tube, a compartment filled with test specimen, to provide optimum positioning of the reference electrode. A counter electrode is used to enable current flow at the working electrode during the test. A graph of the applied potential vs. the measured current is the most useful information that is required in a corrosion measurement. Modern potentiostats enables to program the test cell in a way to continuously apply a varying potential to the working electrode starting from an initial potential and ending at a final potential. The gradual variation in the potential is called a scan and the rate at which the potential is changed is called scan rate. The scan rates can be varied typically from 0.1mV/s to 10mV/s. The data plot obtained, the applied potential vs. current (log of current) can be used to observe passivation phenomena, pitting tendencies or assess the corrosion rate.

Different techniques like Tafel plot, polarization resistance, potentiodynamic anodic polarization, cyclic polarization, potentiostatic, galvanostatic, are employed to measure the corrosion response of a material-solution system. The current research uses potentiodynamic anodic polarization technique to evaluate the corrosion response of the TNZT system in different media.

Potentiodynamic anodic polarization technique is used to determine the active/passive characteristics of a given metal-solution system. This technique uses a scan starting at the E_{CORR} and proceeding until the oxidation of the test solution. The scan rate is usually in the range of 0.1mV/s to 5mV/s. Lower scan rates are preferred to obtain reliable data. The plots obtained are applied potential vs. logarithm of measured current density.

In the current study anodic polarization tests were carried out on LENS deposited TNZT, CP Ti and Ti-6Al-4V ELI samples and also on the boride reinforced TNZT samples. The specimens used were in the form of discs with a diameter of $15mm^2$ and were polished to a surface finish of 0.3 μm. The samples were then cleaned ultrasonically and were employed as the working electrode in the test cell. The tests were carried out in two different media, 0.1N HCl and a simulated body solution known as the Ringers solution. The Ringers solution has a composition of NaCl 9g/l, KCl 0.43 g/l, $CaCl_2$ 0.24 g/l, $NaHCO_3$ 0.2g /l [23]. The anodic polarization test was performed from an initial potential of -1.5 Volts to 5 V at room temperature at a scan rate of 0.166 mV/s and the current density was recorded continuously. A saturated calomel electrode was used as a reference electrode and a platinum wire as a counter electrode. The tests were repeated to ensure the reproducibility of the data obtained.

2.2-3 In vitro Testing

2.2-3-1 Cell Culture

Primary rat bone marrow stromal cells were isolated from the femurs of Sprague-Dawley rats (350-500 grams). Briefly, the rats were sacrificed with CO_2 and the femurs were excised. Aseptically, the femurs were cut at both ends and flushed with 5 ml of primary bone media (DMEM with 10% FBS, 50 μg/ml L-ascorbic acid, 10 mM β-glycerol phosphate, 10 nM dexamethasone, 1% penicillin-streptomycin and 0.2% fungizone) using an 18 gauge needle. The bone marrow pellets were broken up by aspirating the pellets up and down using the syringe, and the cells were seeded in T-25 flasks (~1 femur per T-25 flask). The T-25 flasks were incubated overnight at 37°C in 5% CO_2. Cells were rinsed with PBS, and the media was replaced with complete bone media (DMEM with 10% FBS, 50 μg /ml L-ascorbic acid, 10 mM ²glycerol phosphate, 10 nM dexamethasone, 1% penicillin-streptomycin and 0.1% fungizone). The media was changed again after 24 hrs.

After approximately 1 week, the cells were passed. Briefly, cells were detached with trypsin-EDTA, centrifuged at 1000 Gs for 10 min, and resuspended in complete bone media. Cells were seeded into T-75 flasks and passaged (1:3) when cells reached a confluency of ~80%.

2.2-3-2 Cell Seeding

Cells were detached from the T-75 flasks using trysin-EDTA as above. After centrifugation, the cells were resuspended in media to achieve a seeding density of 10,000 cells/cm^2 onto a disk sample. After adding the cell suspension onto each disk, it was placed in the incubator for 6 hours to allow for cell adhesion. Post-incubation, the media was then aspirated to remove any non-adherent cells and the disks were rinsed once with PBS. The disks

were then transferred to 12-well plates and 1000 µl of fresh media was added to each well. Wells in a 12-well plate were used as positive controls and seeded at the same cell density. On Days 3 and 6, the media was changed in each well; conditioned media was stored at -20˚C.

2.2-3-3 Cell Lysing

On Days 3 and 6, disks were treated with 1% 100X Triton, a cell lysing agent. Briefly, disks from each group were rinsed twice with 1000 µl of PBS, and then immersed in 1000 µl of 1% 100X Triton. The disks were placed in the incubator (37˚C, 95% CO_2) for 30 min. Cells grown on the tops of the disks were scraped and the lysate was then pippetted up and down 3-5 times in the well and stored in a -20˚C freezer for later analysis.

2.2-3-4 DNA Assays

A Pico Green assay kit (Molecular Probes, Eugene, OR) was used to quantitatively determine the amount of double stranded DNA which is presented the cells cultured in vitro on the substrates. The frozen lysate samples were thawed at room temperature. After mixing, 100 µl aliquots of each sample were added to 400 µl of 1xTE in a cuvette. Pico Green Reagent Dye solution (500 µl) were added to each cuvette and incubated at room temperature for 2-5 minutes. A blank sample and standards containing concentrations of 0 to 25 ng/ml of calf thymus DNA were used to make a calibration curve. Readings were taken with a fluorometer (VersaFluor Fluorometer, BioRad) with emission wavelength at 480 nm and excitation wavelength of 520 nm.

2.2-3-5 Alkaline Phosphatase Assays

Alkaline phosphatase is an enzyme found in early stage osteoblasts and can be used as an early marker of bone marrow stromal cells into osteoblast differentiation. The quantification of alkaline Phosphatase is achieved by the conversion of p-nitro phenyl phosphate, a colorless substrate, into p-nitro phenol, a yellow-colored substance. The thawed, sonicated and vortexed samples from the cell lysing were also used to determine alkaline phosphatase concentrations. 80 µl aliquots from each sample were added to individual wells in a 96-well plate with 100 µl of substrate solution (4 mg/ml) and 20 µl of alkaline buffer (1.5 M 2-amino-2methyl-1-propanol at a pH of 10.3). The plate was then incubated for 1 hr at 37^0 C. After incubation, 100 µl of 0.3 N NaOH was added to each well to stop the reaction and the plate reader (UV max kinetic micro plate reader, Molecular Devices) was used to determine the absorbance at 405 nm. Samples were compared to p-nitro phenol standards ranging from 0 to 500 µM.

2.3 Characterization Techniques

2.3-1 Scanning Electron Microscopy

In this study scanning electron microscopy (SEM) was used to characterize the Ti alloys after corrosion and also was used to characterize the wear tracks after the wear tests to understand the wear mechanisms.

Principle:

In the SEM the area to be analyzed is irradiated with a fine beam of electrons generated by an electron gun accelerating them to a high voltage of 0.1-30 KeV. The electrons thus generated are made to raster across the area to be examined after being demagnified. Different types of signals are produced by the interaction of these electrons with the sample surface which includes secondary electrons, backscattered electrons, characteristic X-rays and other photons of

various energies. These signals can be used to examine many characteristics of the sample including surface topography, crystallography, composition etc. The electronics of the detector system are so designed to collect these signals and convert them to produce an image. Secondary and backscattered electrons are the two types of signals most often used to produce SEM images. The standard Everhart-Thornley (E-T) detector collects both the secondary and backscattered electrons. Electrons collected by the scintillator are then amplified for display on the viewing CRT. A vacuum level of 10^{-8} to 10^{-9} is maintained in the electron column with the help of appropriate pumps. With the advent of newer technologies like field emission guns, instrumental resolution of 1-5nm can be achieved in the current instruments.

The instrument that was used in this study was a Nova 200 Dual beam SEM with a field emission gun with a unique capability of a focused ion beam and also a Quanta SEM a high-performance scanning electron microscope, with three modes (high vacuum, low vacuum and ESEM) to accommodate the widest range of samples of any SEM system. The SEM systems are equipped with analytical systems, such as energy dispersive spectrometer. In addition the Quanta 600 is equipped with a backscattered detector to obtain good quality backscattered images. The images were captured at 5-20KV with different spot sizes to obtain the best resolution.

2.3-2 X-Ray Photo Electron Spectroscopy

Surface analysis by X-ray photoelectron spectroscopy (XPS) also known as electron spectroscopy for chemical analysis (ESCA) is done by irradiating a sample with monoenergetic soft X-rays and analyzing the energy of the electrons emitted. MgKα X-rays (1253.6 eV) or AlKα X-rays (1486.6 eV) are generally used. These photons interact with the surface atoms

owing to photoelectric effects and result in the generation of electrons. The kinetic energy of the emitted electrons are given by

$$KE = h\upsilon\text{-}BE\text{-}\varphi$$

Where hυ is the energy of the photon, BE is the binding energy of the atomic orbital from which the electron originates and φ is the spectrometer work function. The BE is regarded as the ionization energy of an atom for a particular shell involved. The electrons leaving the sample are detected by an electron spectrometer according to their kinetic energy. The analyzer operates as an energy window, accepting only those electrons with that energy range, fixed within the window to pass through. This is referred to as the pass energy. Different energy scanning is accomplished by applying variable electrostatic field, before they reach the analyzer. Electrons are detected as discrete events, and the number of electrons for a given detection time and energy is stored digitally.

The X-ray photoelectron spectroscopic data on the oxide layer subjected to corrosion on the TNZT alloys were obtained from a Thermo VG Scientific ESCALAB MKII spectrometer system using a standard Al-Kα X-ray source at 280W and electrostatic analysis in constant pass energy mode of 200eV for survey scans and 20 eV for regional scans. Argon sputtering was carried out for different time intervals to assess the chemical compositions at these sputtered depths.

2.3-3 Atomic Force Microscopy

Atomic force microscopy can be employed to measure the surface roughness of a material surface. A very sharp tip mounted on a very flexible cantilever beam is scanned on the sample surface at a constant normal load to produce very high-resolution 3D images of the sample surfaces. Forces between the sample and the cantilever may cause the cantilever to bend

or deflect. A detector measures the deflections as the tip is scanned over the sample or the sample under the tip. The measured deflections are sent to a computer to generate a map of surface topography. The deflection of the cantilever is aided by different forces. The force most commonly associated with the AFM is the Van der Waals force, depending on the dependence of this force upon the distance between the tip and the sample there are three regimes, the contact regime, non contact regime and the intermittent contact regime or the tapping mode.

The corroded TNZT sample with the oxide layer was subjected to AFM analysis to assess the surface roughness of the corroded and non corroded surface. A 50μm X 50μm area was scanned with AFM (Nanoscope, Veeco USA). The applied bias voltage applied between the tip and the sample was 11 V and the AFM system was operated under tapping mode using a BS tip.

CHAPTER 3

RESULTS OF CORROSION STUDIES

3.1 Introduction

"The biocompatibility of metallic materials is controlled by the chemical or more precisely the electrochemical interaction that results in the release of metallic ions into the tissue and the toxicology of these released substances" [13]. Also it is required of a biomaterial to have excellent resistance to degradation in the human body environment, making it an inevitable requirement to study the corrosion response of the material being considered as an orthopedic alloy. A detailed understanding of the passive oxide layer formed is gained by combining both electrochemical methods and surface analytical techniques offering an insight into the composition, thickness and structure of the oxide layer. Corrosion properties of the Laser Engineered Net shaping™ (LENS) laser based manufacturing solution (Sandia Corp., Albuquerque, NM www.sandia.gov) deposited Ti-35Nb-7Zr-5Ta (TNZT) samples were investigated by anodic polarization technique performed under physiological conditions using a simulated body fluid as well as using 0.1 N HCl solution. Commercially used orthopedic alloys viz. Ti-6Al-4V alloy and commercially pure titanium (CP Ti) were also tested for better comparison of the results. A detailed spectroscopic analysis using X-Ray photoelectron spectroscopy was performed on the oxide layer formed on the TNZT alloy. Micro analytical studies were also done on the oxide layer using atomic force microscopy to determine the roughness of the oxide layer.

3.2 Anodic Polarization Measurements

The overall shape of a potentiodynamic anodic polarization curve plotted with potential with reference to a standard electrode against the current density is as shown in Fig. 3.1. The curve is characterized by different regions and its overall shape is an indication of the corrosion behavior of a material in a given test solution. From the polarization curve it is easy to determine whether a material will passivate in the test solution and also the spontaneity of the passivation. The curve can be divided into three regions the active, passive and the transpassive region. In the active state, the current density increases rapidly with increasing potential resulting in the formation of an oxide layer on the surface of the material. In the passive state the increase in current density reduces and stabilizes to a particular level as a result of the protective film that is formed on the surface in the active state. The transpassive region is characterized by an increase in the current density due to the addition of further potential owing to the breakdown of the film. The ability of a material to form a passive film and its stability or in other words its corrosion resistance can be evaluated using the potential and current measurements obtained from the anodic polarization curve. The parameters of interest are the free corrosion potential E_{Corr}, critical potential and current values E_{crit} and I_{crit}, the passivation holding current density I_p and transpassivation potential E_{tp}. The low critical anodic current at the peak of the polarization curve indicates that the specimen passivates quickly and is stable if the passivation holding current density is low. It is inferred that if the E_{tp} is large and lower currents in the passive region indicate that the film has greater stability.

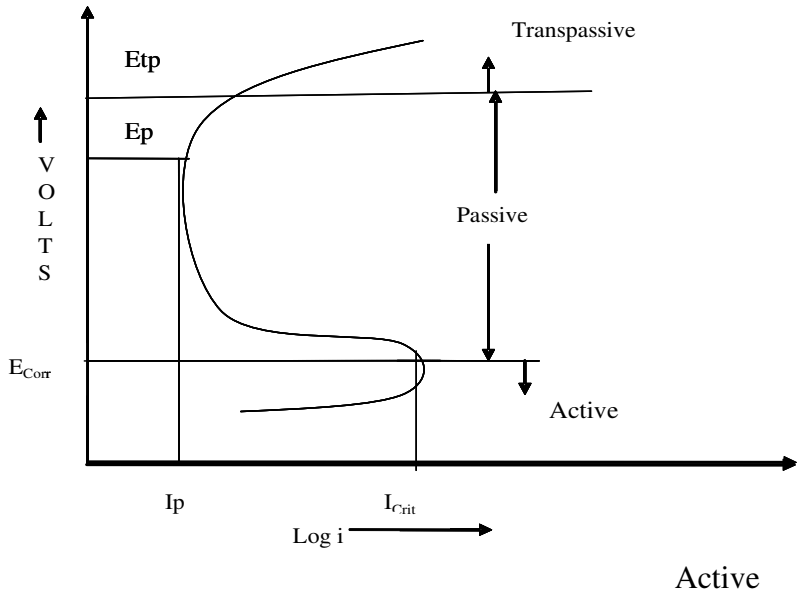

Fig.3.1 Illustration of an anodic polarization curve.

Anodic polarization tests were carried out on CP Ti, Ti-6Al-4V ELI and TNZT in two different test solutions, 0.1 N HCl and Ringers solution. The potential measured with reference to a Saturated Calomel electrode was varied from -2 V to 5 V with a scan rate as low as 0.166 mV/s. Current density was plotted simultaneously and the resulting anodic polarization curve is as shown in Fig.3.2 . All the three materials tested showed a clear active to passive transition at E_{Corr} values close to 0V. There is not much significant difference in the free potential values, E_{corr} for these materials. The active to passive transition exhibited depicts the formation of a passive protective film on the surface of the material. In the case of the conventional alloys Ti-6Al-4V and CP-Ti, the film that forms breaks down at a potential close to 1.5 V while in the case of LENS deposited TNZT alloys the passive film do not show a break down up to a voltage of 5V and above. The critical current density values for CP Ti and Ti-6Al-4V is of the order of 8.4uA/m^2 and 5.3uA/m^2 where as that of TNZT is higher by an order of magnitude, 10.4uA/m^2.

Though the critical current density of TNZT alloys are higher than CP-Ti and Ti-6Al-4V, the Etp or the Transpassive potential for this alloy is higher than 5V , Etp for Ti-6Al-4V and CP Ti being of the order of 1.3 and 1.5 V respectively. This makes the TNZT alloy a better corrosion resistant material in 0.1N HCl when compared to CP-Ti and Ti-6Al-4V.

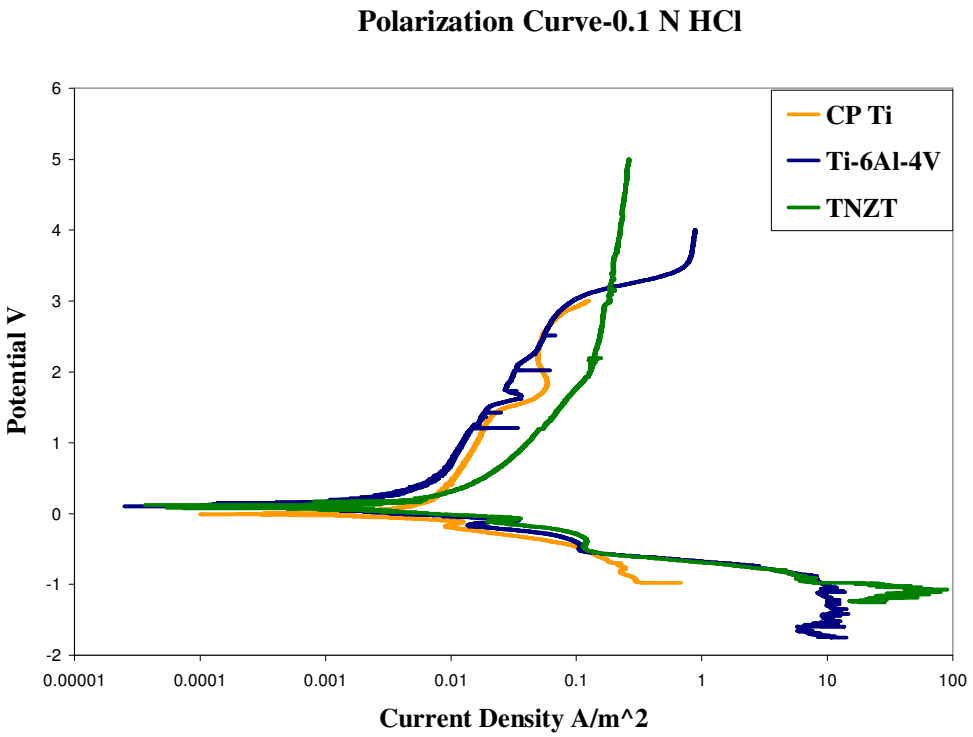

Figure 3.2 Anodic polarization curve for CP-Ti, Ti-6Al-4V ELI and TNZT in 0.1N HCl.

Anodic polarization tests were performed on Ti-6Al-4V ELI, TNZT and TNZT alloy with boride reinforcements in them. The test solution used was a simulated body solution, Ringers solution (NaCl 9g/l, KCl 0.43 g/l, $CaCl_2$ 0.24 g/l, $NaHCO_3$ 0.2g/l) to study the response of these material in a similar condition within the body. Here too as in the case of the previous test described with 0.1N HCl as the test solution the potential measured with reference to a Saturated calomel electrode was varied from -2 V to 5 V with a scan rate as low as 0.166 mV/s.

Current density was plotted simultaneously and the resulting anodic polarization curve is as shown in Fig.3.3. All the three materials tested showed a clear active to passive transition at E_{Corr} values close to 0V. There is not much significant difference in the free potential values, E_{corr} for these materials. The active to passive transition exhibited depicts the formation of a passive protective film on the surface of the material. In contrast to the test in 0.1N HCl, here in Ringers solution all the three materials subjected to testing viz. Ti-6Al-4V, TNZT, and TNZT+2B showed no breakdown of the protective film formed on the surface even at Potentials as high as 5 V. The critical current density value for TNZT alloy (17uA/cm^2) is higher than Ti-6Al-4V by approximately 3 units along the polarization curve. Ti-6Al-4V (14 uA/cm^2) and TNZT+2B (15.36 uA/cm^2) exhibited critical current densities in the same range. The anodic polarization curve shows no breakdown and greater stability of the passive film formed and hence can be inferred that all the three materials tested in Ringers solution are resistant to corrosion and degradation. The typical values of E_{tp} or $E_{br,}$ breakdown potential reported under similar conditions for Stainless steels and Co-Cr-Mo alloys are of the order of 300-500 mV, which can easily be reached in the body in the case of inflammation. [25]. The E_{tp} values for Ti-6Al-4V, TNZT and TNZT+2B are of the order of 5V and hence can be claimed that they have superior corrosion resistance in simulated body fluid conditions.

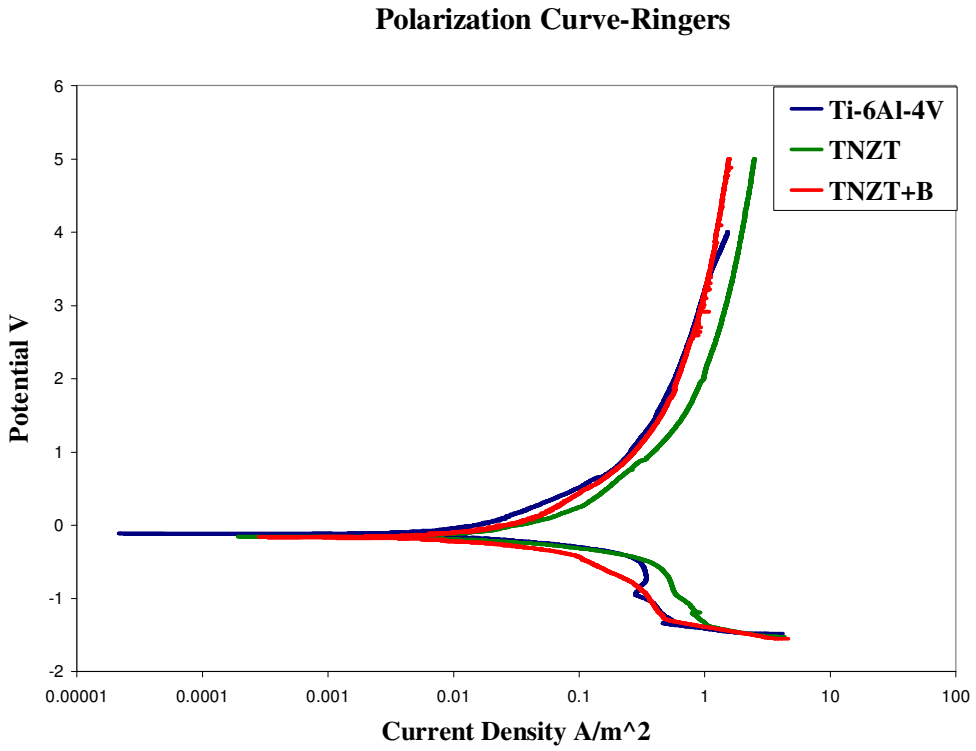

Figure 3.3 Anodic polarization curve for Ti-6Al-4V ELI, TNZT and TNZT+2B in Ringers solution.

3.3 XPS Analysis of the Oxide Surface

The superior biocompatibility and corrosion resistance of Ti alloys are attributed to the stable and dense passive film that forms on the surface in the presence of the oxidizing media. The bio-adhesion of Ti is achieved by free OH^- groups which are available in the pH region from 2.9 to 12.7 on the surface of the oxide layer. These groups react with the bio molecules and are influenced by the chemical and biological characteristics of the surface film. The interaction of the surface oxide film with the bio molecules from the body fluids generates a film called the bio film. The host body initiates a series of reactions in response to this bio film which thereby enable the development of the interface between the implant and the surrounding tissue. Thus it

is important to get a deeper understanding of the oxide film properties like composition, thickness and structure of the oxide layer. The combination of electrochemical methods with surface analytical techniques offers an insight into the understanding of the surface properties of the stable passive oxide layer that is formed on the LENS deposited TNZT alloys by means of anodic polarization. [13]. The oxide layer characterization on electrochemically treated Ti-6Al-4V have been explored by several authors: reports confirm that the surface layer of Ti-6Al-4V comprises mainly of TiO_2 with small amounts of sub oxides TiO and Ti_2O_3. Hence the present study was devoted to analyze the surface oxide layer formed on the LENS deposited TNZT alone which has never been explored before.

As discussed in the experimental chapter of this report, XPS run was carried out on Thermo VG Scientific ESCALAB MKII spectrometer system using a standard Al-Kα X-ray source at 280W and electrostatic analysis in constant pass energy mode of 200eV for survey scans and 20 eV for regional scans. Argon sputtering was carried out for different time intervals to assess the chemical compositions at these sputtered depths. The elements scanned for were C1s, O1s, Ti2p, Nb3d, Ta4f and Zr4f. XPS scans were also performed on the surface of the base material without the oxide layer for comparison. Carbon was a contaminant present and the amount of Carbon decreases with increasing sputtered depth as seen from Fig.3.4.

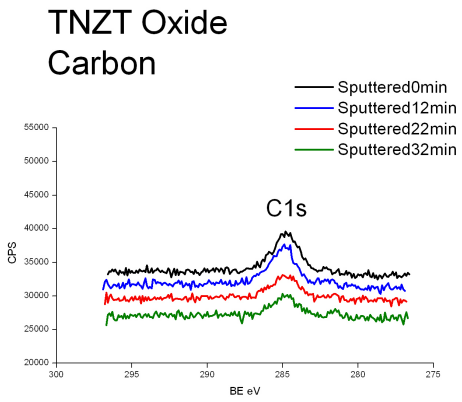

Fig.3.4 XPS spectra for C1s.

In Fig.3.5 XPS spectra of the Ti2p sputtered for a time period of 0minutes, 12 min and 22 minutes on the oxide surface of the TNZT alloy subjected to electrochemical testing and the spectra for the base TNZT alloy without the oxide layer sputtered for a time interval of 30 minutes is represented. As can be observed from the spectra the TiO_2 2p3/2 (Eb=458.4)[26] peak is observed on the surface and as sputtering is done into the oxide layer for 22 minutes the peak corresponding to metallic titanium is observed with a binding energy of Eb=453.7[26]. Also on the base sample after a sputtering of 30 minutes peaks corresponding to metallic titanium is detected. This shows that after about 22 minutes of sputtering the oxide layer is surpassed and are in the base material. Also the presence of TiO_2 even after the sputtering of 22~30 minutes into the base suggests that TiO_2 might have been incorporated from the nascent oxide layer present.

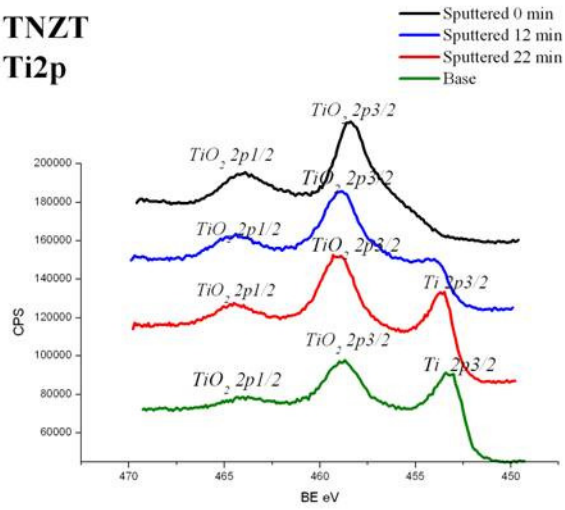

Figure 3.5 XPS spectra of Ti2p on the oxide and base TNZT.

Fig.3.6 represents the XPS spectra of the Nb3d sputtered for a time period of 0minutes, 12 min and 22 minutes on the oxide surface of the TNZT alloy subjected to electrochemical testing and the spectra for the base TNZT alloy without the oxide layer sputtered for a time interval of 30 minutes. The surface of the oxide layers showed the presence of $Nb_2O_5$3d5/2 (207.01eV and an oxy-nitrile of the composition NbN(1-y)O(y) 3d5/2. (Eb=203.6eV). As sputtered inside for 12 minutes and beyond in to the oxide layer oxides other than Nb_2O_5 are detected. NbO_2, NbO0.2Nb and NbO are the other oxides that form along with Nb_2O_5. Metallic Nb peak appears after a sputtering of 22 minutes into the oxide layer and 30 minutes in to the base. As in the case of titanium, niobium oxide peaks are detected in the XPS spectra even after a sputtering of 30 minutes both in the oxide layer and the base layer.

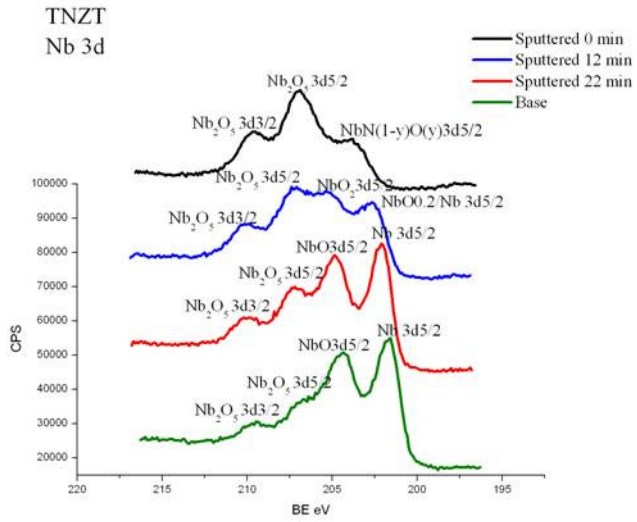

Figure.3.6 XPS spectra of Nb3d on the oxide and base TNZT.

In the case of the elements Zr and Ta XPS spectra was collected for the same conditions as for Ti and Nb as shown in Fig.3.7 and Fig.3.8. In the case of Zr the oxide present was ZrO_2 and as sputtered in to oxide as well as the base layer the presence of metallic Zr was detected with the coexistence of ZrO_2 as seen from Fig 3.7. For Ta, as observed from Fig.3.8 Ta_2O_5 was the form of oxide detected on the surface along with metallic tantalum on the surface of the oxide layer. Thus it can be inferred that the oxide formation tendency of Ta is much less when compared to the other elements viz. Ti, Nb and Zr.

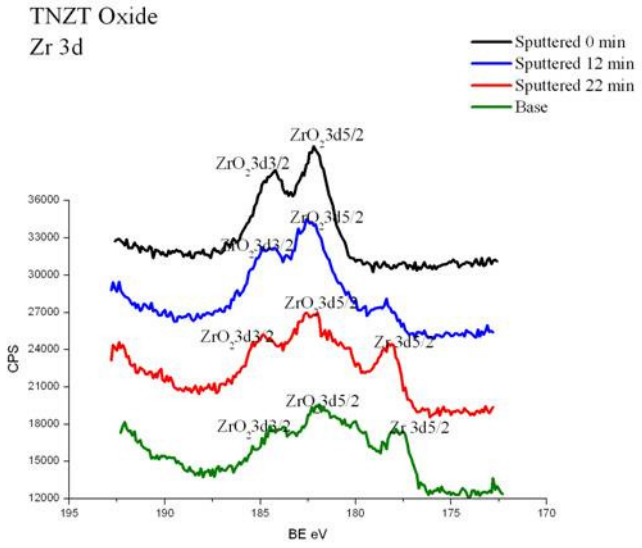

Figure 3.7 XPS spectra of Zr3d on the oxide and base TNZT.

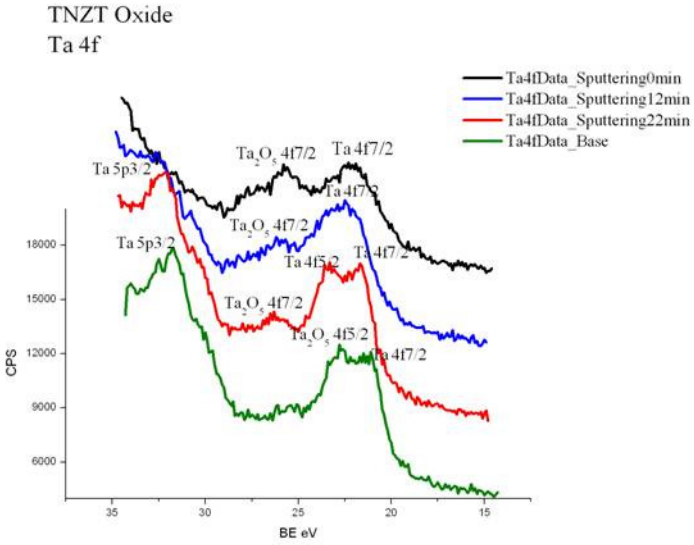

Figure 3.8 XPS spectra of Ta4f on the oxide and base TNZT.

Thus the protective oxide layer formed on the surface of the laser deposited TNZT alloy is a combination of complex oxides of the elements Ti, Nb, Zr and Ta. These oxides are listed in the Table.3.1.

Sputtering Time (min)	Ti Based	Nb Based	Ta Based	Zr Based
0	TiO_2	Nb_2O_5,NbN(1-y)O(y)	Ta_2O_5,Ta	ZrO_2
12	TiO_2, Ti	Nb_2O_5,NbO_2,NbO0.2/Nb	Ta_2O_5,Ta	ZrO_2
22	TiO_2, Ti	Nb_2O_5,NbO,Nb	Ta_2O_5,Ta	ZrO_2,Zr
Base	TiO_2, Ti	Nb_2O_5,NbO,Nb	Ta_2O_5,Ta	ZrO_2,Zr

Table.3.1 Analysis of the XPS spectra.

3.5 AFM Results

In order to obtain more insight into the nature of the oxide film that was formed AFM studies were performed on the electrochemically corroded TNZT layer and the non corroded base layer. It was found that the Z range, Ra and Rq values all indicative of surface roughness was slightly higher for the corroded samples when compared to the non corroded surfaces. The AFM micrographs are presented in Fig 3.9 and Fig 3.10 for the non corroded and corroded surfaces respectively and the values are summarized in Table.3.2 .

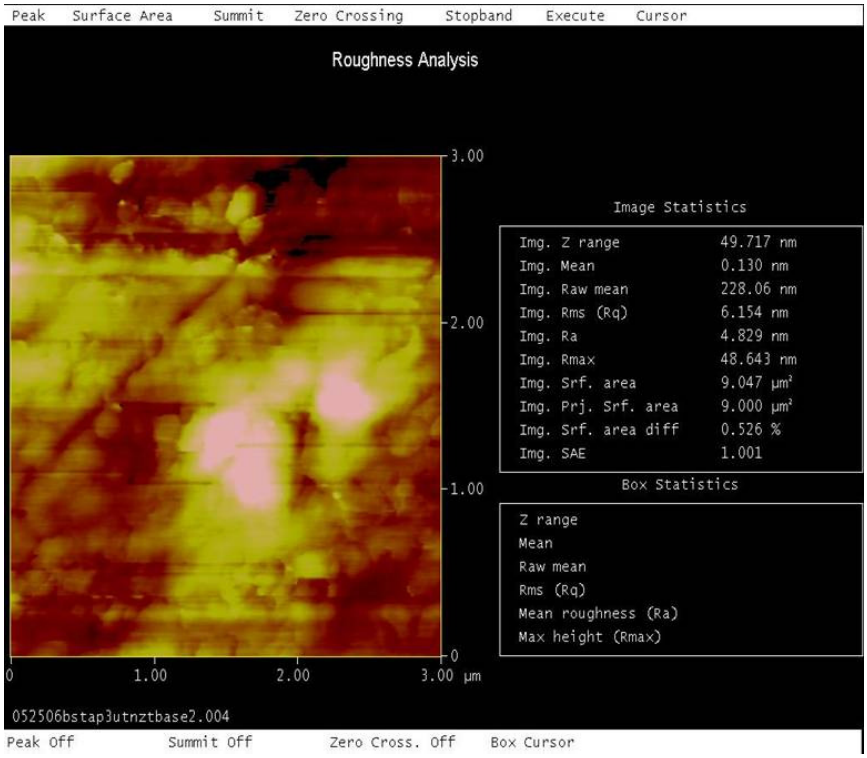

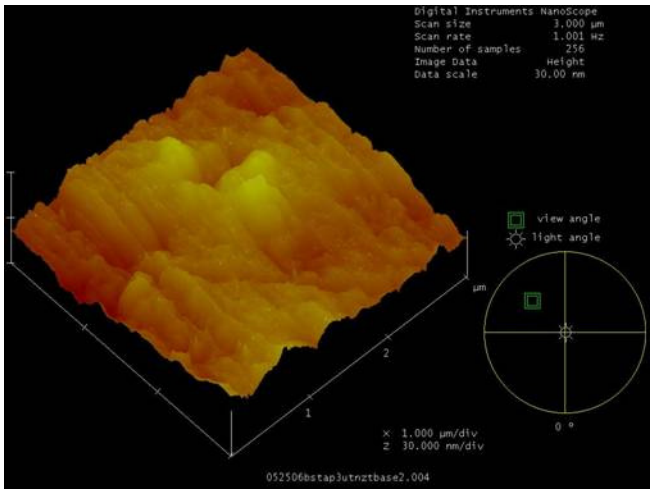

Figure 3.9 Roughness analysis on the non corroded TNZT surface.

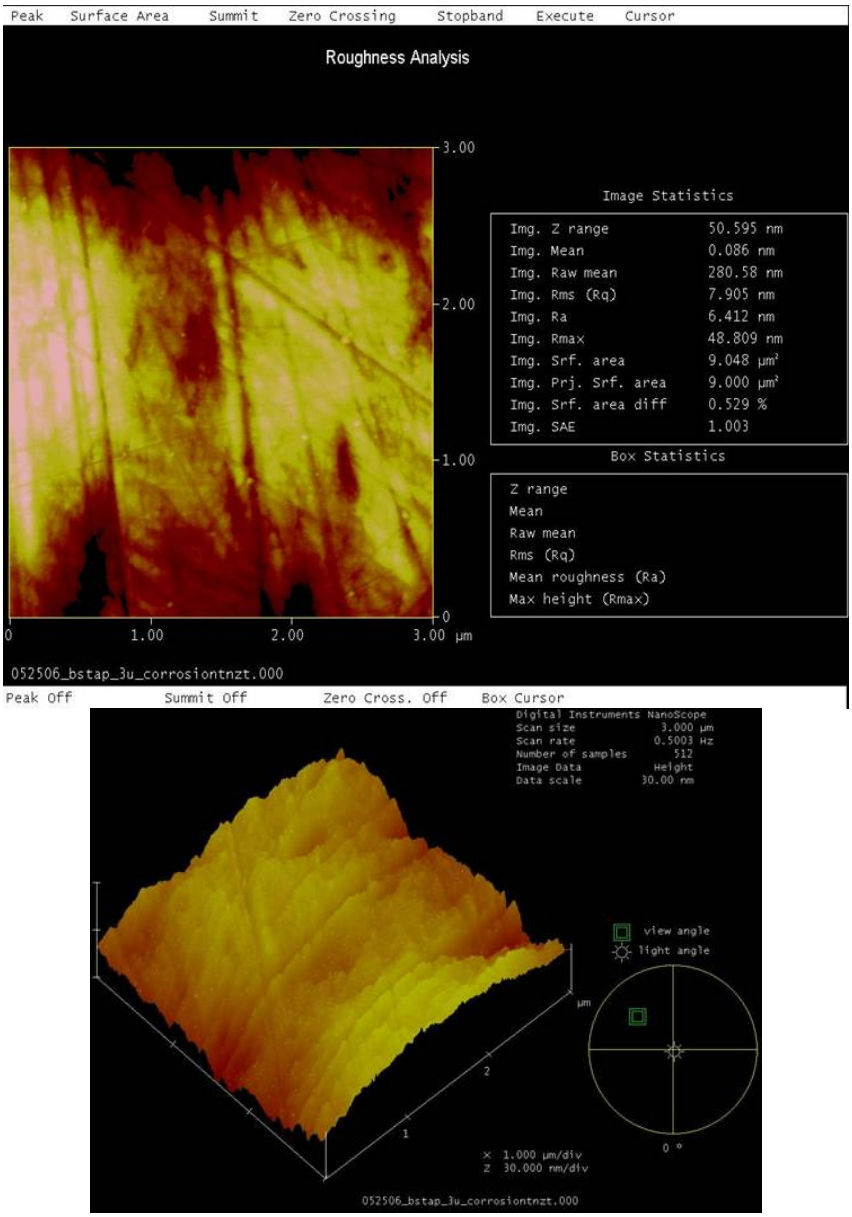

Figure 3.10 Roughness analysis on the corroded TNZT surface.

	Non Corroded	Corroded
Z Range (nm)	49.7	50.59
Rq (nm)	6.15	7.9
Ra	4.82	6.4

Table.3.2 Analysis of the AFM data.

CHAPTER 4

RESULTS OF IN VITRO STUDIES

Bone formation is a complex process involving the migration of bone cells to the bone surfaces termed as bone proliferation of the osteoprogenitor cells and their subsequent differentiation into osteoblasts. Hence assessing the extent of bone proliferation and bone differentiation on the surface of a material of interest is a method to evaluate its biocompatibility. In this study primary rat bone marrow cells isolated from the femurs of Sprague Dawley rats were seeded in T-75 flasks and subsequently incubated. Seeded cells were then detached and resuspended in media to achieve a seeding density of 10,000 cells /cm2 and added on to the Ti-6Al-4V and Ti-35Nb-7Zr-5Ta (TNZT) disk samples. Following this the disks were incubated for 6 hours to allow cell adhesion. The disks were then transferred to well plates used as positive controls. After the 4th and the 7th day or (3^{rd} and the 6^{th} day) the disks were treated with a lysing agent and cells grown on top of the disks were scraped and the lysate was pippetted out. A Pico green assay kit was used to quantitatively determine the amount of double stranded DNA present in the cultured cells. Alkaline phosphate an enzyme found in early stage osteoblasts was used as an early marker of bone marrow stromal cells into osteoblast differentiation. This experiment was repeated twice to ensure the reproducibility in the test results.

In the first set of data obtained as shown in Fig.4.1 it was observed that rate of bone proliferation measured as a function of the amount of DNA present in the cultured cells was higher in the case of laser deposited TNZT alloys when compared to the control Ti-6Al-4V ELI after 4 days. However after 7 days both the Ti-6Al-4V and TNZT exhibited almost the same rate of bone proliferation. The rate of bone differentiation studied using Alkaline

Phosphate enzyme as a marker showed a significant amount of ALP enzyme in the TNZT sample when compared to the Ti-6Al-4V indicating enhanced bone differentiation after a period of 7 days. As can be seen from the Fig.4.2. The amount of ALP enzyme that was present in the case of Ti-6Al-4V was relatively lower than that of the TNZT sample. This definitely suggests that the laser deposited TNZT alloys are biocompatible as they aid bone cell proliferation and differentiation.

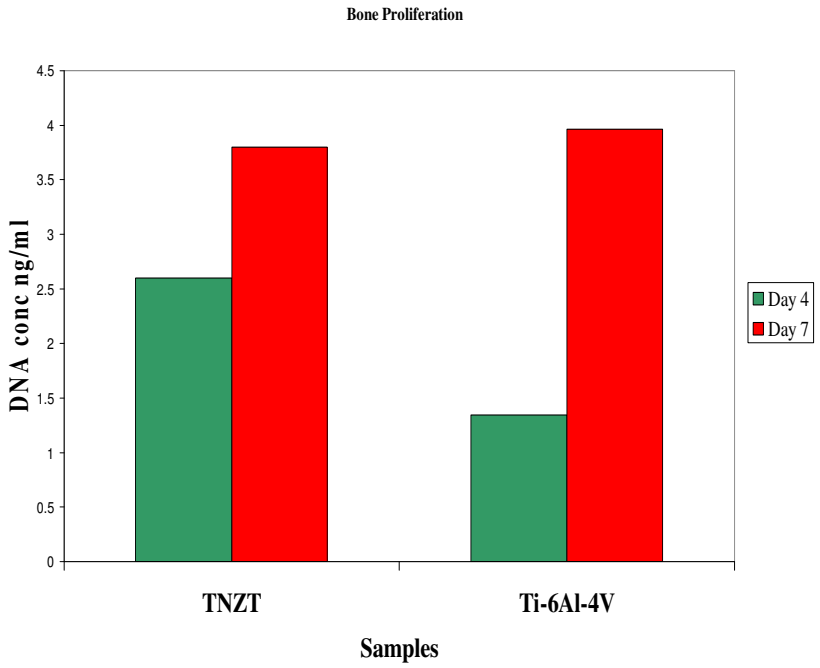

Figure 4.1 Bone cell proliferation.

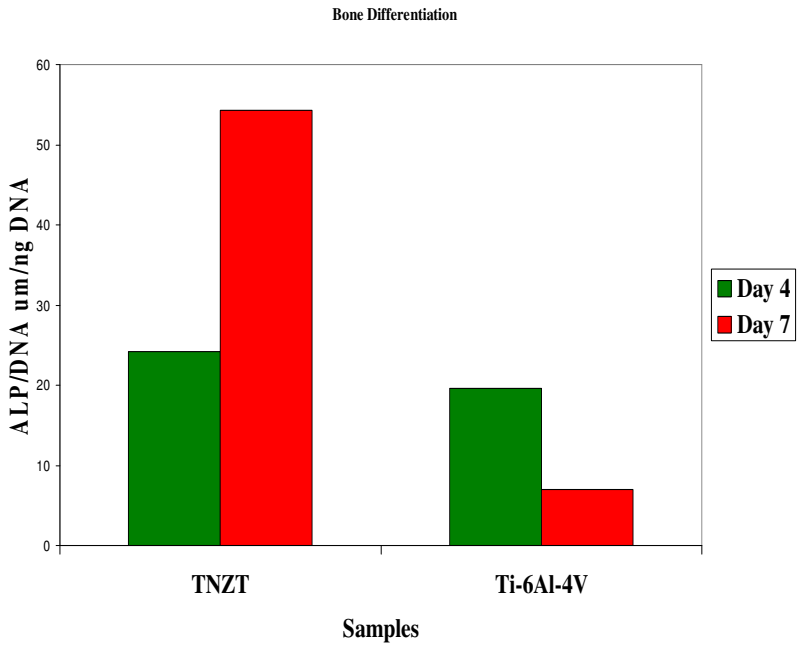

Figure 4.2 Bone cell differentiation.

The second sets of experiments were also done under similar conditions as the first set the data from these experiments are represented as shown in Fig.4.3 and Fig.4.4. The PicoGreen DNA assays (Invitrogen) are used to measure Total DNA concentration, which is correlated to the cell number grown on the surfaces. Studies of DNA were performed after 3 and 6 days of bone cell seeding. The results are presented as follows in Fig. 4.The ALP assays are used to measure the ALP production per ng DNA for each sample used to indicate the bone cell differentiation. It was observed that the TNZT samples enhance more bone cell differentiation for bone marrow stem cells compared to the Ti-6Al-4V ELI controls. In contrast, cell growth in TNZT samples is not as good as those grown on control samples in this second set of data collected. These results suggest that the Ti-35Nb-7Zr-5Ta alloy promotes the osteogenic potential of bone marrow stem cells compared to the traditionally used Ti-6Al-4V alloy.

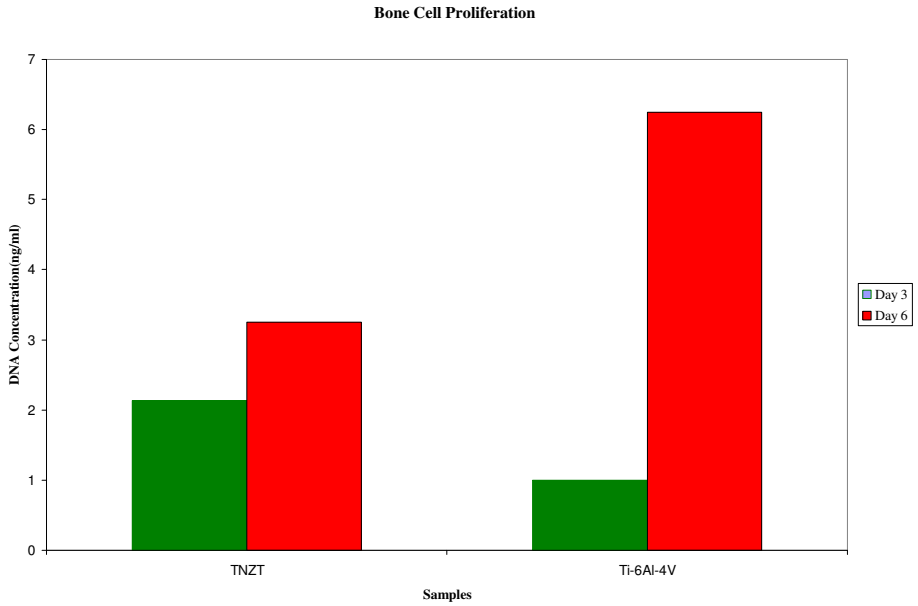

Figure 4.3 Bone cell proliferation for the second data set.

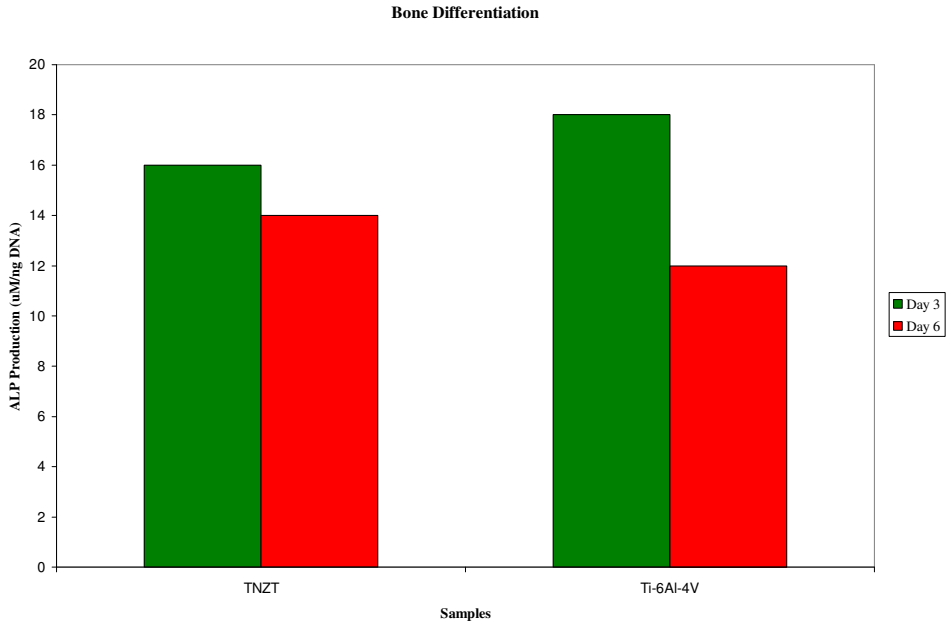

Figure 4.4 Bone cell differentiation second data set.

In addition, the results have large deviation compared to cells grown on tissue culture plates. This may be due to the cell spilling when seeding on the Ti samples. It is recommended

that a barrier be build around the samples to avoid spillage of he tissue culture medium to avoid deviation in the data. Sketch of barrier is shown as in Fig.4.5.

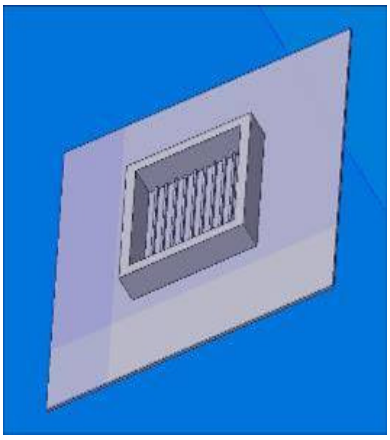

Figure 4.5 Sketch of a sample with a barrier proposed for future study.

CHAPTER 5

BORIDE REINFORCEMENTS IN THE Ti-35Nb-7Zr-5Ta (TNZT) MATRIX

5.1 Introduction

In recent years, there has been a considerable amount of research devoted to the development of TiB reinforced Ti-alloy composites. These composites combine the high strength and stiffness of the borides with the toughness and damage tolerance of the Ti-alloy matrix and offer attractive properties including increased stiffness and substantially enhanced wear resistance [17]. Using the Laser Engineered Net shaping™ (LENS) laser based manufacturing solution (Sandia Corp., Albuquerque, NM www.sandia.gov) process, it has been successfully demonstrated that in situ TiB reinforced Ti alloy composites can be fabricated in a single step. These laser-deposited composites exhibit a substantially refined microstructure as compared to their conventionally processed (e.g. ingot processing) counterparts. Furthermore, as discussed previously, since biomedical implants are geometrically quite complex, by employing novel near-net shape processing technologies, LENS it is possible to not only rapidly and efficiently manufacture custom-designed implants but also functionally-grade them to exhibit required site-specific properties. Therefore, the current effort is directed towards the laser-deposition of boride reinforced TNZT composites based on the nominal matrix composition Ti-35Nb-7Zr-5Ta (all in wt %).

5.2 Microstructural Evolution

The microstructure of the LENS deposited sample at different magnifications is shown in the backscatter Scanning electron microscope (SEM) images in Fig. 5.1. Fig 5.1(a) shows a low magnification backscattered image of the boride composite. Higher magnification micrographs

as seen in Fig 5.1(b) show that the microstructure consists of the coarser primary boride precipitates and the finer scale eutectic boride precipitates dispersed in a matrix. Furthermore, while the finer scale eutectic borides exhibit a uniform contrast in the backscatter SEM images, the coarser primary boride precipitates exhibit strong contrast variations within the same precipitate suggesting a possibility of compositional variation within the same boride. In addition, the matrix also exhibits variations in contrast. Thus, while the regions adjoining the primary boride precipitates exhibit a lighter contrast, the regions a further distance exhibit a relatively darker contrast. There is also a clustering of the eutectic boride precipitates within these regions of darker contrast, as clearly visible in Fig. 5.1(b). SEM-Energy dispersive spectroscopy (EDS) studies revealed that the composition of the matrix to be Ti-34%Nb-7%Zr-7%Ta (all in wt %). Fig. 5.2 shows the results of EDS studies carried out on one of the primary boride precipitates. The SEM image of the specific boride precipitate analyzed is shown in Fig. 5.2(a) together with the line across which the compositional variation was measured using SEM-EDS. The compositional profile across this line is shown in Fig. 5.2(b) and has been divided into distinct zones within the boride precipitate, exhibiting the different contrasts in Fig. 5.2(a). On either sides of the boride, the composition of the matrix is Ti-33Nb-7Zr-9Ta which is marginally enriched in Ta as compared with the average alloy composition (~ 7 wt% Ta). The relatively higher Ta content of the matrix in the vicinity of the primary boride precipitates is also indirectly indicated by the lighter contrast in these regions (adjacent to the primary borides) seen in the SEM backscatter image in Fig. 5.1(b). Within the boride precipitate, there are distinct alternating bands of dark and bright contrast. It should be noted that in the profile shown in Fig. 5.2(b), the composition of the boride does not include the boron content (since it cannot be quantified by EDS) and has been scaled to Ti+Nb+Zr+Ta = 100 wt%. The average composition of the matrix

adjacent to the boride is Ti-33Nb-7Zr-9Ta (all in wt %). The boride precipitate can be divided into five distinct composition zones based on the bands of different contrast visible in Fig. 5.2(a). In Fig. 5.2(b), Zone I corresponds to the first band and exhibits a continually decreasing Ti and Zr content while the Nb and Ta contents increase. In Zone II, the composition appears to be nominally constant and approximately equal to Ti-40Nb-4Zr-16Ta. However, it should be noted that the composition of these bands might not be constant along the direction normal to surface. Therefore, it is not possible to accurately determine the composition of these bands using SEM-EDS but rather use these measurements as a qualitative indicator. In band III, the Nb and Ta contents increase while that of Ti and Zr decreases. The reverse trend is observed in case of band IV, wherein Ti and Zr increase while Nb and Ta decrease. Finally, band V exhibits the same trend as band III. Overall the compositional changes in these bands within the boride precipitate appear to follow an alternating trend of increasing and decreasing Ti and Zr (or decreasing and increasing Nb and Ta).

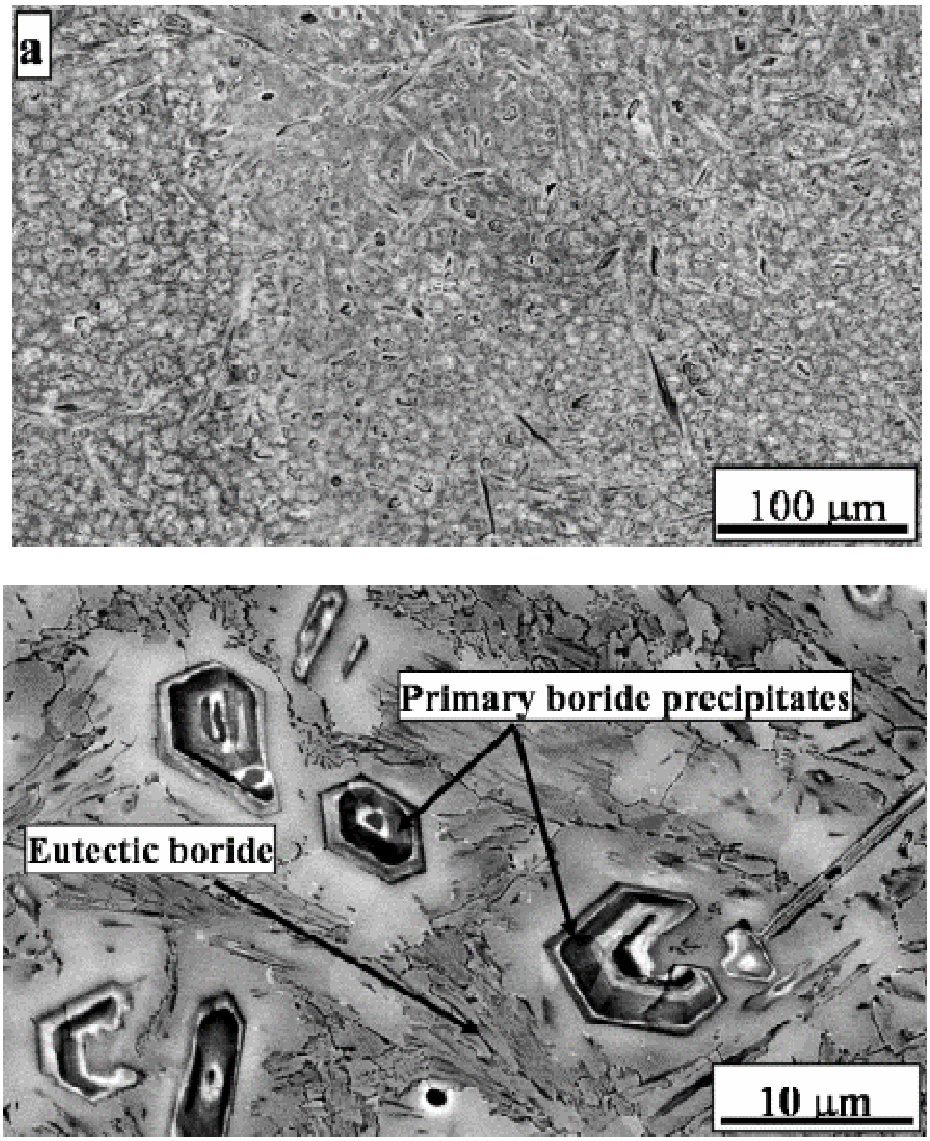

Figure 5.1 a and b SEM backscattered images of boride precipitates in the TNZT matrix.

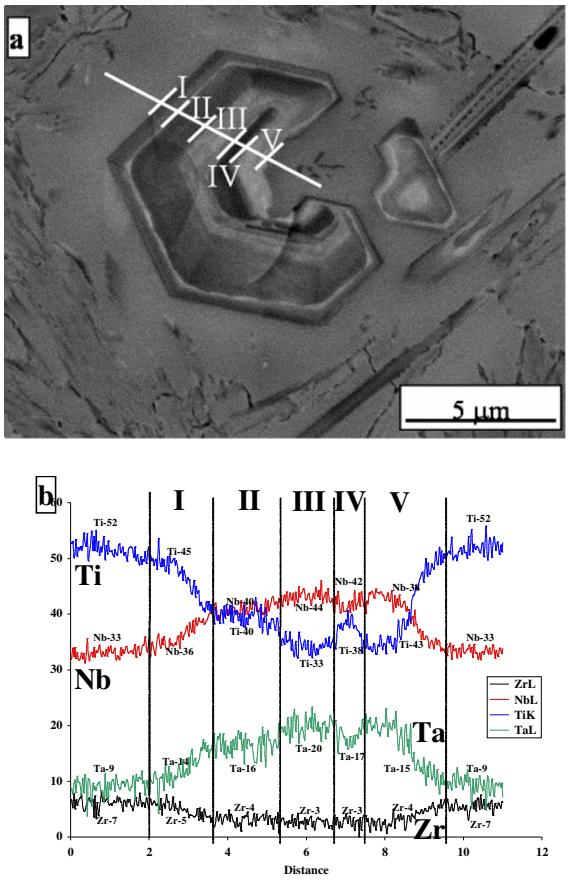

Figure 5.2 SEM backscattered image of the boride precipitate and their compositional modulation.

CHAPTER 6

RESULTS OF WEAR STUDIES

6.1 Introduction

Owing to the site specific requirements in an orthopedic implant alloy, it is important that a material being considered for use in a site where there is a lot of wear involved should possess good wear resistance. The reinforcement of borides in a Ti matrix has been the subject of study for quite some years now and the results show that these borides reinforced composites exhibit superior tribological response. The reinforcement of these harder precipitates can be facilitated by using novel net shaping technologies like Laser Engineered Net shaping™ (LENS) laser based manufacturing solution (Sandia Corp., Albuquerque, NM www.sandia.gov). The Ti-35Nb-7Zr-5Ta (TNZT) base matrix with the borides has many advantages such as it become possible to get a much refined microstructure when compared to the conventionally processed alloys, the processing can be done in a single step and can be custom designed, also the site specific requirements can be met by functionally grading the alloys. Therefore, the current effort is directed towards the laser-deposition of boride reinforced TNZT composites based on the nominal matrix composition Ti-35Nb-7Zr-5Ta (all in wt %). Thus, the need to study the fundamental tribological properties and mechanisms of these next generation alloys before application is addressed in this chapter. Sliding wear resistance and friction behavior was examined under a wide range of post processing and testing conditions such as varying the concentrated interfacial load, the effect of ex situ annealing on the tribological properties, and the role of counterpart material. Correlating the tribological properties to the surface microstructure was also studied under these conditions.

Friction and wear behavior of TNZT, TNZT+2B and Ti-6Al-4V ELI (Extra Low Interstitial) were determined using a Falex (Implant Sciences) ISC-200 Tribometer. The counterface materials chosen were Si_3N_4 (H= 1550 HV/10) and SS 440 C (H= 420 HV/10) balls of 1.6 mm radius. These counterpart materials chosen are harder than the metallic samples as seen from Table 6.1. Also SS440 balls have lesser hardness values when compared to Si_3N_4 balls. The two counterpart materials were chosen to facilitate to compare the friction response of these metallic samples with a relatively softer and harder counterface. Tests were performed at a constant normal load of 5 N which corresponds to the initial mean Hertzian contact stress (p_m) values listed in Table 6.1. The friction coefficients were calculated throughout the test by taking the ratio of the tangential load, measured by a strain gauge transducer, to the normal load. The tests were performed up to 10,000 sliding cycles at a tangential sliding velocity of 46 mm/s, which lies in the range typically found in hip joints [24], In addition, the tests were run at room temperature in open air with a relative humidity of ~35 %. Before testing the 15 mm diameter alloy surfaces were polished to # 1200 SiC followed by fine polishing up to 0.05 μm colloidal silica. Also, some of the polished samples were subjected to separate heat treatments in air before testing, shown in Table 6.2. The objective of the TNZT+2B and the Ti-6Al-4V ELI alloy heat treatments were two fold, to study the influence of α precipitates and the influence of the oxide layer, formed as a result of the heat treatment, on the friction and wear behavior.

Alloy	Hardness(VHN)	p_m (GPa) for Si3N4 balls	p_m (GPa) for SS 440 C balls
Ti-6Al-4V ELI	320	0.95	0.90
TNZT 2B	375	1.01	0.95
TNZT	280	0.67	-

Table 6.1: Hardness and initial mean Hertzian contact stresses (p_m) for Ti-6Al-4V ELI, TNZT 2B and TNZT.

ALLOY	**HEAT TREATMENT**
Ti-6Al-4V ELI	As deposited
Ti-6Al-4V ELI	600^0 C/10hours/FC/Oxide Layer
Ti-6Al-4V ELI	600^0 C/10hours/FC/Oxide Layer removed
TNZT 2B	As deposited
TNZT 2B	600^0 C/10hours/FC/Oxide Layer
TNZT 2B	600^0 C/10hours/FC/Oxide Layer removed

Table 6.2: Heat Treatment conditions for Ti-6Al-4V and TNZT 2B for wear testing.

6.2 Friction and Wear Results

6.2-1 Friction Results of the As-Deposited Alloys

Typical friction curves are shown in Fig. 6.1 for as-deposited Ti-6Al-4V ELI, TNZT and TNZT+2B sliding against Si3N4. The friction coefficients immediately increased to high values of ~0.4 and 0.5 for Ti-6Al-4V, TNZT and TNZT+2B, respectively. With continued sliding, their steady-state friction coefficients leveled off at ~0.5 and 0.6, respectively, for Ti-6Al-4V and

TNZT 2B for the reminder of the tests. In the case of TNZT the coefficient of friction values scaled even higher to the order of 0.7~0.8. The friction behavior observed in these alloys can be well correlated to the micrographs of the Wear tracks in Fig. 6.2. As can be observed in the case of Ti-6Al-4V ELI, the low and high magnification images of the wear track show evidence of surface deformation due to ductile layering and smearing, common in repeated sliding contacts for Ti-6Al-4V alloys [17]. TNZT exhibits much severe abrasive wear, as can be evident from Table1. the base TNZT alloy has much lesser hardness of the order of 280 VHN, when compared to the higher hardness values of Ti-6Al-4V ELI and TNZT 2B which are of the order of 320 and 375 VHN respectively. The hardness values correspond to the mean pressure between the surface and the ball and since the mean pressure value is much lower than compared to the other two materials it can be inferred that TNZT is bound to exhibit a much aggressive wear. The TNZT+2B wear track morphology shown in Fig 6.2 exhibits less severe wear than compared to the TNZT matrix but much severe wear when compared to Ti-6Al-4V ELI. Owing to the presence of the high hardness and the presence of the harder TiB precipitates the TNZT 2B is expected to exhibit a much milder wear and a low friction coefficient when compared to Ti-6Al-4V. The higher COF value and the severe wear when compared to Ti-6Al-4V ELI came as a surprise and was the subject of investigation.

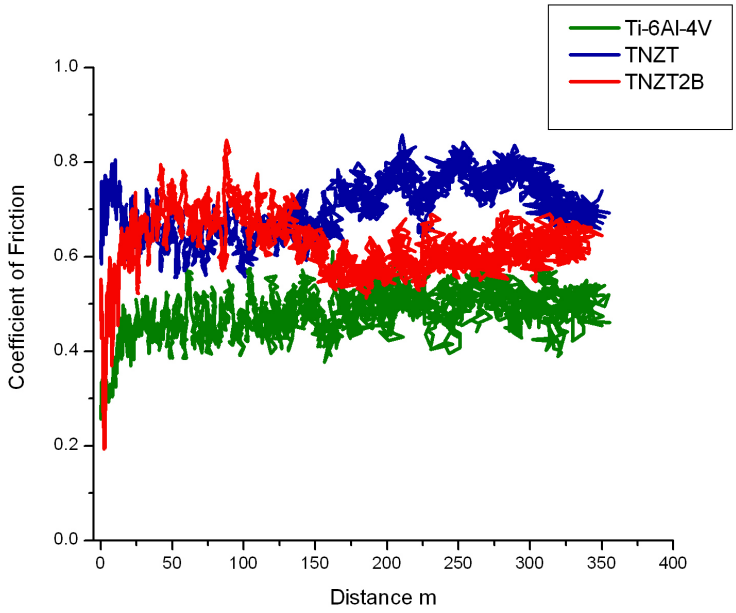

Figure 6.1 Friction behavior of Ti-6Al-4V ELI, TNZT, TNZT 2B tested against Si3N4 balls under room temperature conditions.

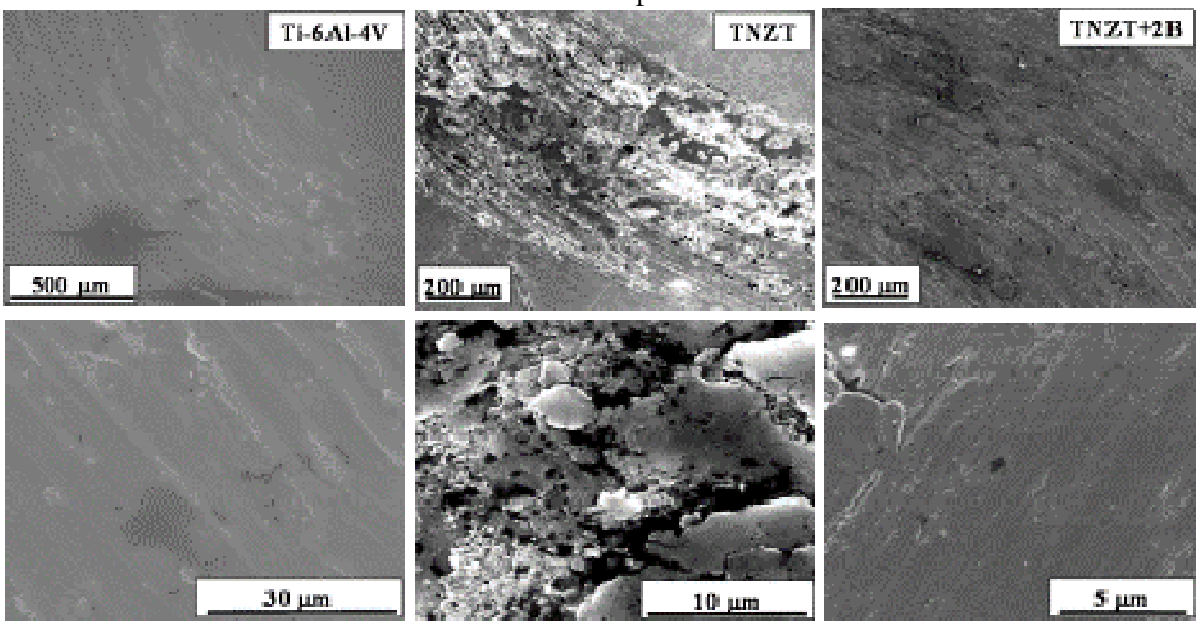

Figure 6.2 SEM wear tracks of Ti-6Al-4V, TNZT, TNZT 2B tested against Si_3N_4 at room temperature.

One possible explanation for this behavior is the pull-out of the harder TiB precipitates from the matrix resulting in third body wear, which would accelerate abrasive wear events by

ploughing and deep grooving, as shown in Fig. 6.2. Hence further SEM studies were carried out to establish this explanation. The SEM image captured in the immediate vicinity of the wear track shown in Fig. 6.3 confirms that one of several TiB precipitates (~10 μm on edge) being pulled-out of the matrix inside the wear track, which is in agreement with previous observations of boride pull out from the matrix of Ti-6Al-4V reinforced with TiB_2 reported by De Hosson et. al. [17]. From these results it was surmised that the hard Si_3N_4 ball, much harder than would be active in a hip prosthesis contact, was responsible for precipitate pull-out from the Ti-6Al-4V matrix. The next step adopted in the course of the study was to perform heat treatments to study the influence of the presence of α precipitates on the softer β TNZT matrix of the TNZT+2B sample. For the sake of comparison similar heat treatment was carried out on Ti-6Al-4V ELI. Samples were heated to 600^0 C in air and held for 10 hours and then furnace cooled. The influence of the oxide layer on the tribological response of the alloys was also studied. The study was the confined mainly to TNZT 2B and Ti-6Al-4V ELI as TNZT base alloy showed a much severe wear when tested with Si_3N_4 conditions.

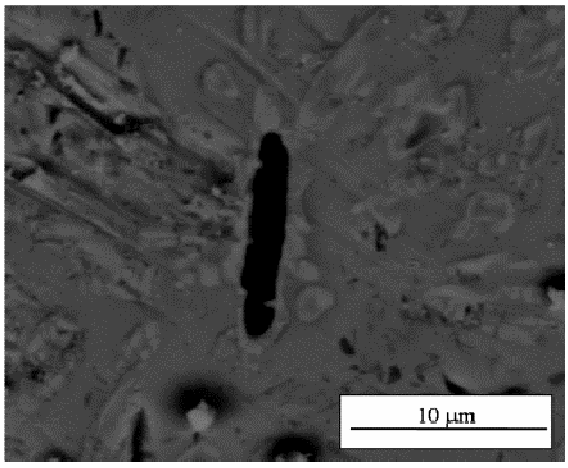

Figure 6.3 Boride pullout from a TNZT 2B alloy tested against Si_3N_4.

6.2-2 Friction Results on the Oxide Layer of the Heat Treated Samples

The heat treated samples with the oxide layer were subjected to friction testing. Prior to the friction testing the oxide surface of the TNZT+ 2B sample was characterized with the help of a high resolution SEM as shown in Fig.6.4 and Fig.6.5. The sample was imaged at both lower and higher KV using secondary electrons. The boride precipitates appeared as though they were etched by the oxide layer. The image that was obtained using higher KV showed much less contrast between the borides and the matrix, where as the one obtained using lower KV showed much higher contrast that the eutectic and primary borides could be distinguished. The α precipitated owing to its fine size could not be resolved through the oxide layer.

Figure 6.4 SE Image at high KV of the oxide layer on the heat treated TNZT2B.

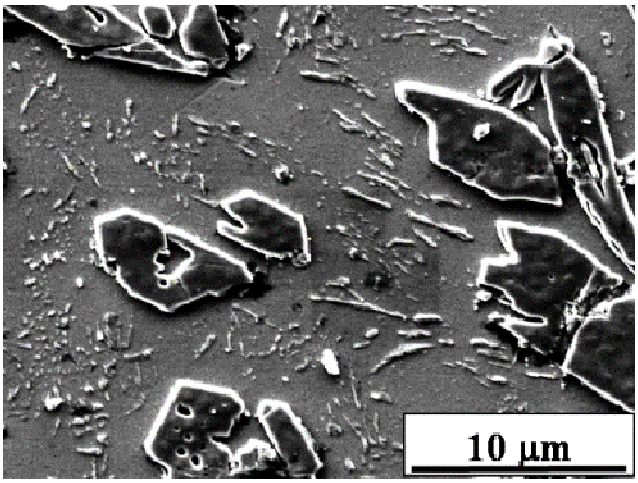

Figure 6.5 SE image at Low KV of the oxide layer on the heat treated TNZT2B.

Trenches were made on the oxide surface to roughly estimate the thickness of the oxide layer formed as shown in Fig.6.6. From the micrographs the oxide layer thickness was estimated

to be roughly of the order of 30 nm, which confirmed to previous studies on the oxide layer formed on β Ti alloys. [14]

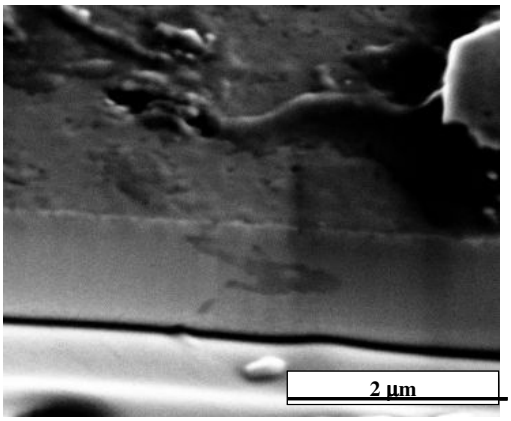

Figure 6.6 Trench made on the Oxide layer of heat treated TNZT+2B.

Friction testing was done on heat treated Ti-6Al-4V ELI and TNZT 2B with the oxide layer intact to study the influence of the oxide layer. Friction coefficients as seen from Fig.6.7 of the alloys sliding against Si_3N_4, are much lower than the non-oxidized alloys. After an initial run-in period, the steady-state friction coefficients are ~0.23 and 0.17 out to 80 m sliding distance for Ti-6Al-4V ELI and the TNZT+2B, respectively. These are very low friction coefficients typically exhibited for oxidized titanium materials [14]. In addition, these friction coefficients show much less fluctuations compared to their as-synthesized state suggesting a more stable sliding interface without debris in the contact. The values are also consistent with the corresponding wear track morphologies shown in Figs. 6.8 and 6.9. Based on these SEM images, both wear track morphologies exhibit a change in mechanism to mild oxidative wear, which suppresses the previous plastically dominated wear mechanisms shown for the as-synthesized alloys. The toughened titanium oxide layers, likely the rutile phase, showed much narrower wear tracks with no significant third body debris formation that would result in severe

abrasive wear. This shows that the titanium oxide layer acted as a lubricous oxide and prevented boride particles from being potentially pulled out of the matrix, and thereby improved the wear resistance considerably for both Ti-6Al-4V ELI and TNZT+2B. Lubricous oxides, such as rutile, have been shown to be very effective in lowering the friction coefficients (~0.2) and wear rates [27]. Lastly, there were no significant differences in the wear track morphologies between the alloys outside of some patchy regions in TNZT+2B that did not contribute to the overall friction behavior.

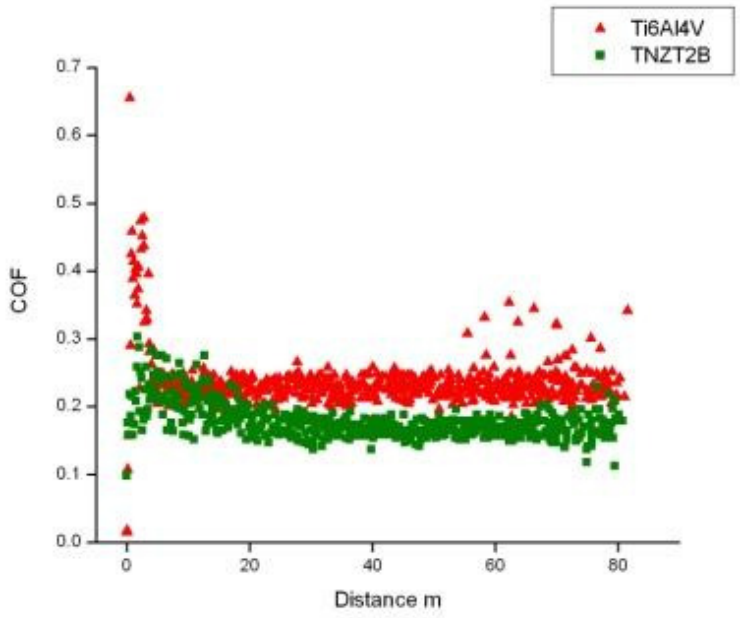

Figure 6.7 Friction behavior of Ti-6Al-4V ELI and TNZT 2B with the oxide layer tested against Si_3N_4 balls under room temperature conditions.

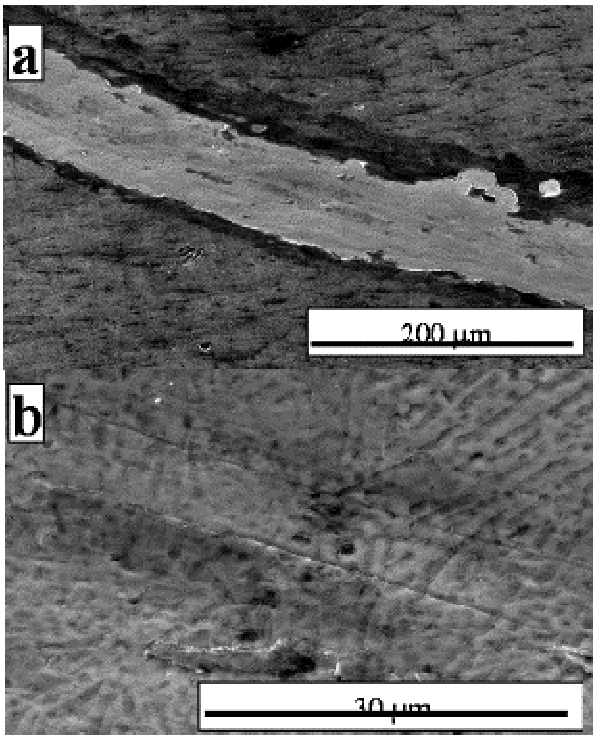

Figure 6.8 SEM images of wear tracks of Ti-6Al-4V ELI with the oxide layer on Si_3N_4 balls (a and b).

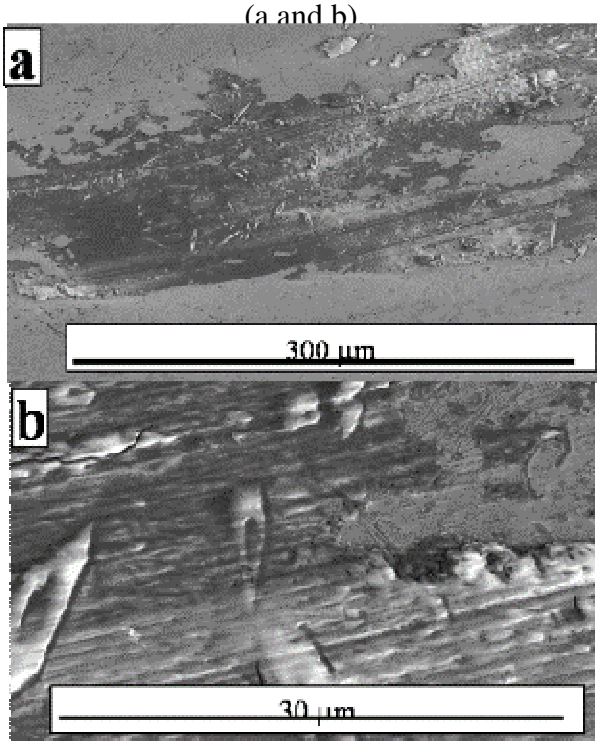

Figure 6.9. SEM images of wear tracks of TNZT 2B with oxide layer on Si_3N_4 balls (a and b).

The next step adopted was to evaluate the friction and wear behavior when the TNZT+2B microstructure was returned to the as-synthesized state. This was done by heating the TNZT+2B sample to 900^0 C a temperature well above the β transus and holding at this temperature for 1 hour and then subjecting to a rapid cooling by immediately quenching the sample in water. The sample was then examined in the SEM to make sure that it was free of α precipitates. Here instead of using the harder Si_3N_4 (H~1550 HV/10), sliding was carried out against a softer couterface material, SS440C (H~420 HV/10) in Table 6.1. This contacting condition would be more representative of an actual ball and socket joint. Fig.6.10 shows typical friction coefficient curves for the alloys sliding against a SS 440C counterface ball after removal of the oxide layers by a light polish. The initial friction coefficients of both Ti-6Al-4V and TNZT+2B are approximately of the order of 0.1; however the friction coefficient of Ti-6Al-4V after a sliding distance of ~15m showed an increase. A continual steady increase in the friction coefficient occurs up to ~0.4 to 0.6, similar to the values shown in the as-deposited condition in Fig. 6.1. These higher and more fluctuating values suggest increased abrasive wear and debris generation. In contrast, the initial friction coefficient of TNZT+2B alloy remained at a very low steady-state value of ~0.13 for the entire test, instead of the high values (~0.6) shown in Fig. 6.1 for the as-synthesized condition. Thus, the softer steel counterface eliminated the TiB precipitate pull-out, third body abrasive wear observed with the harder Si_3N_4 counterface. The corresponding SEM images of the wear tracks shown in Figs. 6.11 and 6.12 for Ti-6Al-4V ELI and TNZT+2B, respectively, corroborate the friction behavior. The wear track morphology of Ti-6Al-4V ELI in Fig.6.11 shows more extensive plastic deformation, microplowing and cutting all typical processes associated with an abrasive wear mechanism. Conversely, the TNZT+2B wear track shown in Fig. 6.12 exhibits less severity in wear. It is apparent the surface morphology has

undergone a plastic shear deformation mechanism usually associated with less wear volume removal. This is evident by examining some of the larger surface depressions with plastic flow process. These results show much lower friction coefficient and improved wear resistance can be obtained by using a softer counterface material when returning to the TNZT+2B as-synthesized state, much lower than observed for current Ti-6Al-4V ELI alloys.

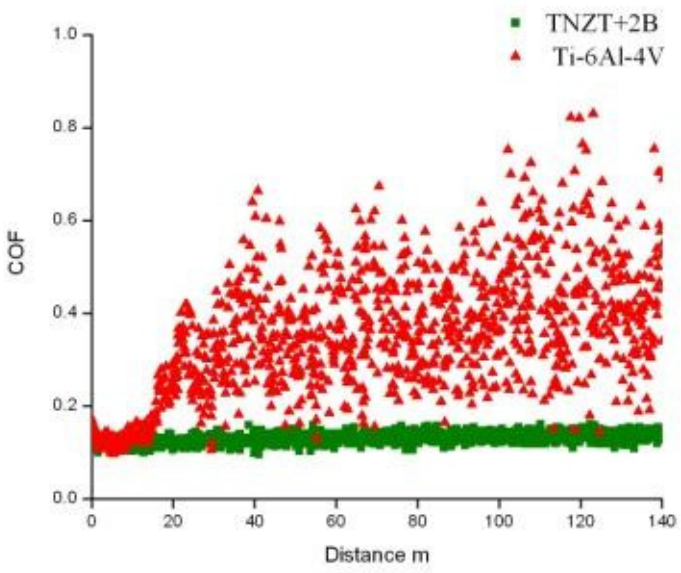

Figure 6.10 Friction behavior of Ti-6Al-4V ELI and TNZT 2B with SS440C balls in as-synthesized condition.

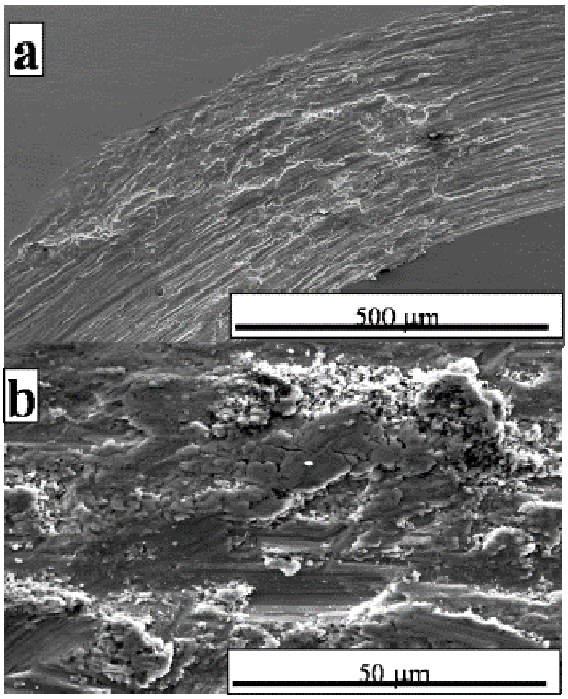

Figure 6.11 SEM images of as deposited Ti-6Al-4V ELI wear tracks with SS440 C balls (a and b).

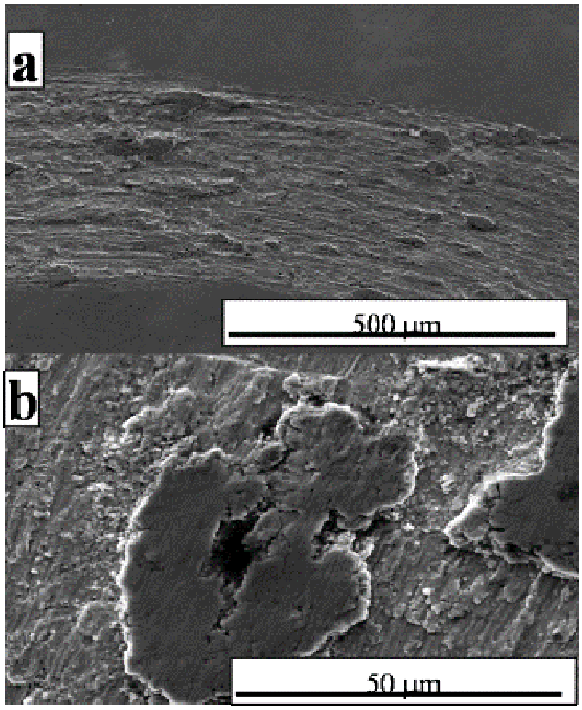

Figure 6.12 SEM images of as deposited Ti-6Al-4V ELI wear tracks with SS440 C balls (a and b).

CHAPTER 7

CONCLUSIONS

Novel net shaping technique Laser Engineered Net shaping™ (LENS) laser based manufacturing solution (Sandia Corp., Albuquerque, NM www.sandia.gov) can be used to deposit orthopedic implant alloys. Ti-35Nb-7Zr-5Ta (TNZT) alloy system was deposited using LENS. One of the prerequisites for a material to be used as an implant material is that it should possess superior corrosion resistance. Hence the corrosion resistance of the LENS deposited TNZT alloy was tested electrochemically and was found to be better than the conventionally used Ti-6Al-4V ELI in both 0.1N HCl and a simulated body solution (Ringers solution).A detailed analysis of the oxide layer formed from corrosion exhibited the presence of complex oxides which are responsible for the excellent corrosion resistance. The TNZT alloy was also subjected to In vitro testing and the results are quite promising indicating excellent biocompatibility measured in terms of the proliferation and differentiation of rat bone marrow cells, seeded on the metal surfaces.

In order to improve the wear resistance of the TNZT system boride reinforcements were carried out in the matrix using LENS processing .The boride precipitates in as deposited LENS TNZT+2B contain compositionally segregated regions of higher Ti (Zr) or Ta (Nb) weight percent. The tribological response of the metal matrix composites was studied under different conditions and compared with Ti-6Al-4V. Usage of Si_3N_4 balls as a counterpart in the wear studies showed that there is boride pullout resulting in third body abrasive wear with higher coefficient of friction (COF). Using 440C stainless steel balls drastically improved the COF of as deposited TNZT+2B and seemed to eliminate the effect of “three body abrasive wear”, and also exhibited superior wear resistance than Ti-6Al-4V.

The influence of oxide film was also evaluated and it was seen that oxide film improves the wear resistance of both TNZT+2B and Ti64.

REFERENCES

1. M. Long and H.J Rack, Biomaterials 19 (1998) 1621.
2. Yale Medical Group. May 9, 2007.http://ymghealthinfo.org/content.asp?pageid=P00068
3. S.Nag, R.Banerjee, H.L Fraser, Mat.Sci.Eng.C 25 (2005) 357.
4. K. Wang , Mat.Sci.Eng.A 213 (1996) 134
5. T. Ahmed, M.Long, J. Silvestri, C.Ruiz, H.J Rack, titanium '95 Science and Technology, Birmingham (1996) 1760.
6. D. Kuroda, M. Niinomi, M.Morinaga, Y.Kato, T. Yashiro, Mat.Sci.Eng.A243 (1998) 244.
7. US Food and Drug Administration. May 9, 2007 http://www.fda.gov/cdrh/recalls/zirconiahip.html
8. About: Arthritis, May 9, 2007 http://arthritis.about.com/library/weekly/aa012001a.html
9. Brown Nealy." Sulzers new problem: Knee replacements" St. Petersburg Times, June 1 2001, May 9, 2007 http://www.sptimes.com/News/060101/TampaBay/Sulzer_s_new_problem_.shtml
10. K.I Schwender, R.Banerjee, P.C.Collins, C.A. Brice, H. L. Fraser, Scripta. Mater. 45 (2001) 1123.
11. R.Grylls, Adv.Mater.Process. 161 (1) (Jan 2003) 45.
12. R. Banerjee, S.Nag, S.Samuel, H.L Fraser J. Biomed. Mater. Res A 78 (Aug 2006) 298.
13. H.Zitter, H.Plenk Jr, J. Biomed. Mater. Res Vol 21 (1987) 881.
14. D. Velten, K. S. Meuser, V. Biehl, H. Duschner, J. Breme. Z. Metallkd. 94 (2003) 667.
15. Y.L Zhou, M. Niinomi, T. Akahori, H. Fukui, H. Toda. Mat.Sci.Eng.A 398 (2005) 28.

16. K.Wang, L. Gustavson, J. Dumbleton . Beta titanium alloys in the 1990s. The minerals, Metals & materials society (1993). 49

17. V. Ocelik, D. Mathews, J.Th.M.De Hosson, Surf.Coat.Tech 197 (2005) 303.

18. M. Long, H.J. Rack. Wear 249 (2001) 158

19. S.J.Li, R.Yang, S.Li, Y.L. Hao, Y.Y. Cui, M. Niinomi, Z.X. Guo, Wear 257 (2004) 869.

20. M. Niinomi, T. Hanawa, T. Narushima, J.Mater. Sci.57 (4) (Apr 2005) 18.

21. M. Niinomi, Biomaterials 24 (2003) 2673.

22. J.Dolder, A.J.E Ruijter, P.H.M.Spauwen, J.A.Jansen, Biomaterials 24 (2003) 1853.

23. L.Thair, U. Kamachi Mudali, R Asokamani and Baldev Raj, Mater. Corros. 55. No.5 (2004), 358.

24. M.P Gispert, A.P Serro, R Colaco, B Saramago Wear 260 (2006) 149.

25. J.H Zitter, J.Plenk J.Biomed.Mater.Res.21 (1987) 881.

26. NIST Homepage. May 9, 2007 http://srdata.nist.gov/xps/

27. M.N. Gardos, Trib. Lett. 8, (2000) 79.